

Preliminary Studies of Scalar Transport in Turbulent Jets

Using Point-Particle DNS Simulations

by

Venkata Sai Sushant Paturu

A Thesis Presented in Partial Fulfillment
of the Requirements for the Degree
Master of Science

Approved July 2023 by the
Graduate Supervisory Committee:

Gokul Pathikonda, Chair
Mohamed Housseem Kasbaoui
Jeonglae Kim
Prasanth Prabhakaran

ARIZONA STATE UNIVERSITY

August 2023

ABSTRACT

The current work aims to understand the influence of particles on scalar transport in particle-laden turbulent jets using point-particle direct numerical simulations (DNS). Such turbulence phenomena are observed in many applications, such as aircraft and rocket engines (e.g., engines operating in dusty environments and when close to the surface) and geophysical flows (sediment-laden rivers discharging nutrients into the oceans), etc.

This thesis looks at systematically understanding the fundamental interplay between (1) fluid turbulence, (2) inertial particles, and (3) scalar transport. This work considers a temporal jet of Reynolds number of 5000 filled with the point-particles and the influence of Stokes number (St). Three Stokes numbers, $St = 1, 7.5, \text{ and } 20$, were considered for the current work. The simulations were solved using the NGA solver, which solves the Navier-Stokes, advection-diffusion, and particle transport equations.

The statistical analysis of the mean and turbulence quantities, along with the Reynolds stresses, are estimated for the fluid and particle phases throughout the domain. The observations do not show a significant influence of St in the mean flow evolution of fluid, scalar, and particle phases. The scalar mixture fraction variance and the turbulent kinetic energy (TKE) increase slightly for the $St = 1$ case, compared to the particle-free and higher St cases, indicating that an optimal St exists for which the scalar variation increases. The current preliminary study establishes that the scalar variance is influenced by particles under the optimal particle St . Directions for future studies based on the current observations are presented.

ACKNOWLEDGMENTS

I consider myself fortunate to pursue my master's project under the guidance and supervision of Professor Gokul Pathikonda. I am also grateful for the allocation of the project, imparting me with knowledge along with continual motivation and support during the hard times. His constant feedback, suggestions and discussions have all given me the research acumen I have gained during this period.

I would also like to thank Professor Mohamed Housseem Kasbaoui and his PhD student Shuai Shuai for their continuous help and support in understanding and debugging the NGA repository on which the simulations are carried out. Their clarity and knowledge of the repository have greatly helped me understand the coding aspects and helped me to develop suitable code for the project simulations.

I would also like to thank my thesis panel committee members – Prof. Gokul Pathikonda, Prof. Mohamed Housseem Kasbaoui, Prof. Jeonglae Kim and Dr Prasanth Prabhakaran for not only their time and patience but also for their intellectual contributions to the development of my thesis work. Their vast amount of knowledge and experience helped my thesis project to grow into a masterpiece.

I would also thank my teammates at ASU's Complex Mixing and Advance Turbulence Laboratory and my friends for their constant support, brainstorming and motivation during the critical times of debugging and building the customized code required for my project. I would also like to thank my academic advisor – Ya Hu, for the advice regarding the doubts that I have in academic stuff.

I would also like to thank the Mechanical Engineering Department at Arizona State University for giving me an opportunity to pursue research in fluid mechanics, one of my fields of interest. I would also thank the ASU research Computing group for providing me with a suitable number of computational cores (resources) for performing the DNS analysis for various cases within the stipulated time.

I would also like to thank the developer of the VisIt, a data visualization and analysis tool that is used in this work along with the MATLAB, for taking their busy time out and helping me in solving my doubts that I have regarding various options and the instructions to get the desired output results from the VisIt software.

On a personal note, I am thoroughly indebted to the continual selfless love and support from my parents throughout the entire duration of my master's program. Without them, my master's career and completion wouldn't be a reality.

TABLE OF CONTENTS

	Page
LIST OF FIGURES	vi
LIST OF FIGURES	viii
CHAPTER	
1. INTRODUCTION	1
Definitions	1
Literature Review	3
Current Work	7
2. SIMULATION DETAILS	8
Introduction	8
Governing Equations	10
Solver Algorithm	13
Meshing and Grid Parameters	15
Initial and Boundary Conditions	16
3. SIMULATION INPUTS	17
4. RESULTS & DISCUSSIONS	19
Simulation Analysis	19
Qualitative Analysis in Streamwise-Normal Plane	19
Statistical Analysis in Streamwise-Parallel Plane	22
Statistical Analysis in Streamwise-Normal Plane	31

CHAPTER	Page
Qualitative Analysis of Particles Clustering	50
Statistical Analysis of Spread Rates	55
5. CONCLUSIONS & FUTURE WORK	57
REFERENCES	62

LIST OF FIGURES

Figure	Page
2.1.1 – Different Approaches to Turbulent Multiphase Flows	08
2.1.2 – Common Methods Used in Turbulence Simulations	09
4.2.1 – Jet Mixture Fraction Profiles in the Span-wise Direction for Different St and at Different t_e	20
4.2.2 – Jet Velocity Profiles in the Span-wise Direction for Different St and at different t_e	21
4.3.1 – Mean of Mixture Fraction over Time for Various St	22
4.3.2 – Variance of Mixture Fraction over Time for Various St	23
4.3.3 – Spanwise Velocities of the Jet Fluid for Various St over Time	24
4.3.4 – Velocity Variance of the Jet in (a) Streamwise, (b) Cross-stream, and (c) Spanwise Directions, for Different St over Time	25
4.3.5 – Turbulent Kinetic Energy of the Jet (TKE_f) for Various St over Time	27
4.3.6 – Spanwise Velocities of the Particles for Various St over Time	28
4.3.7 – Velocity Variance of the Particles in (a) Streamwise, (b) Cross-stream, and (c) Spanwise Directions, for Different St over Time	29
4.3.8 – Turbulent Kinetic Energy of Particles (TKE_p) for Various St over Time	30

Figure	Page
4.4.1 – Mean of Mixture Fraction over Time for Different St	31
4.4.2 – Variance of Mixture Fraction over Time for Different St	34
4.4.3 – Spanwise Velocities of the Jet Fluid for Different St	37
4.4.4 – Variance of the Jet Velocity in Streamwise Direction for Different St	39
4.4.5 – Variance of the Jet Velocity in Cross-stream Direction for Different St	41
4.4.6 – Variance of the Jet Velocity in Spanwise Direction for Different St	43
4.4.7 – Turbulent Kinetic Energy of the Jet (TKE_f) for Different St	46
4.4.8 – Co-variance ($u'_f v'_f$) of the Fluid for Different St	48
4.5.1 – Single Layered Particle Plot Overlaid on Fluid Velocity for $St = 1$	51
4.5.2 – Single Layered Particle Plot Overlaid on Fluid Velocity for $St = 20$	52
4.5.3 – Single Layered Particle Plot Overlaid on Mixture Fraction for $St = 1$	53
4.5.4 – Single Layered Particle Plot Overlaid on Mixture Fraction for $St = 20$	54
4.6.1 – Time Series of Jet Velocity Half-width for Different St	55
4.6.2 – Time Series of Jet Concentration Half-width for Different St	56

LIST OF TABLES

Table	Page
3.6.1 – Configurations of the DNS Simulations for Different St	18

INTRODUCTION

1.1 – Definitions

Turbulence is a common phenomenon that occurs commonly in natural phenomena, and in engineering and industrial applications. It can be described as the unsteady, irregular, random, and chaotic fluid flow that is observed in the surroundings (Pope, 2000). Hinze (1975) describes turbulence as “An irregular flow condition in which various quantities show a random variation with time & space coordinates”. Although the concept of turbulent flows has been commonly known for a long time, the understanding of the turbulent flow, its quantitative analysis and estimation is still an active area of research. The main reason for it is the presence of the inertial term in the Navier Stokes equation which requires closure schemes to solve (Foias et al, 2001).

One of the major ways in which the turbulence is generated is at the wall or by the flow of layers of fluids with different velocities past one another. This is called turbulent shear flow (JO Hinze, 1975). There are 3 major types of turbulent shear flows – (1) Homogenous Turbulent Shear Flow, (2) Wall-bounded Turbulent Shear Flow and (3) Free Turbulent Shear Flow (Atta et al., 1995). The free turbulence shear flow occurs between two streams of differing velocity generating velocity gradients between them with no direct effect of the boundaries. The free shear flows are mainly composed into three types – (1) Jets, (2) Wakes and (3) mixing layers (Hinze, 1975).

The turbulent jets are the most studied to understand the behavior of the free shear flows. In jets the turbulence occurs due to the mean-velocity difference between the two

fluid media without the interference of the boundary walls (Pope, 2000). Depending on the inlet type, the jets can mainly be classified into 2 types – (1) axisymmetric (or) round jets, and (2) planar jets. As the name suggests, the round jet is a type of jet flow in which the fluid enters the domain through inlet (or) nozzle area. Since the jet inlet is boundless in all the three directions, the jet is free to expand in all the three directions. This is different in comparison with planar jets. As the name suggests, planar jets have an inlet opening that isn't bounded in one cross-sectional direction. Here, in these jets, the fluid comes out from the long length (typically the infinite) along one of the cross-sectional axes of the jet. The variation (or) the velocity gradient along the above discussed cross-sectional axis is very low (close to 0) in comparison with the gradients in other directions, making the fluid to freely expand in the latter directions only.

The other method of classifying the jet flows is through the jet evolving methods in space and time. Here also, the jet flows are typically classified into 2 types – (1) Spatial jets, and (2) Temporal jets. The difference between these two types of jet is their evolution of velocity gradients in space and time planes. For the spatial jets, the jet evolution (or) the change in overall velocity is observed in the special direction(s) and being stationary in the temporal domain whereas for the temporal jets, the jet evolution (or) the change in overall velocity is observed in the temporal domain, making it independent of the spatial direction(s). In the temporal jets case, the jet is assumed with certain initial condition of jet flowing inside the domain in contrast with the spatial jet case, in which the jet is assumed to start from the nozzle area and make it through the other end of the domain. The most common jet profile that can be possible to experiment with is the spatial jet. Hence more

of the past and ongoing research is done in the domain of spatial jets in comparison with the temporal jets.

For the current work, we consider turbulent temporal plane jets that is laden with particles. There can be two types of particles flowing in the domain – (1) Passive flow of the particles, and (2) Inertial flow of the particles. Passive particles are the category of particles which don't cause significant momentum or energy difference between themselves and the fluid flow. These particles typically tend to replicate the fluid flow properties. Whereas the inertial particles are the category of particles that cause momentum and energy difference between themselves and the fluid flow. These particles typically tend to modify the flow propagation. The main variable that determines if the particles behave as active (or) passive is the Stokes number, St . St is the ratio of particle response time to the fluid response time. If a St is low, then the particle's response to change with the fluid is extremely high in comparison with the fluid response giving the particles least resistance to change the flow. The reverse happens at high St , making the particles give resistance to the fluid flow for the response. This makes the case with low St as passive particles flow and the case with high St as active particles flow.

1.2 – Literature Review

The earliest computational model that was developed to understand the turbulence and mixing phenomenon in jets was by Corrsin & Kistler (1955). They have conducted experiments and built models to understand the mixing between the turbulent and non-turbulent boundary layer. This means that the focus was on the boundaries of the jet and its mixing into the static fluid domain around the jet. From this point on, most of the research

started to grow in the turbulence jets along with understanding the mixing of the jet into the surroundings along with the fluid transport process across them.

During the early research on the particle-laden jets, various experiments were undertaken like – particles in liquids and gases, drops or sprays in liquids and gases, and bubbles in liquids to understand the impact of particles on the fluid flow and the turbulence mixing between the jet and stationary domain (Parthasarathy et al., 1987). Also, the interaction between the solid particles with the turbulent flow was examined through the behavior of particles in a jet dominated by vortex ring structures (Longmire et al., 1992). These early models have based their simulation on the data obtained from the experiments.

The earliest $k - \epsilon$ models were proposed by Elghobashi (1984), in which the turbulence kinetic energy and its rate of dissipation were modelled along with the time-averaged turbulent correlations. The simulation was considered for a coarser mesh grid, and the jet considered was the turbulent axisymmetric gaseous jet with spherical uniform-sized solid particles. The same kind of setup was also used for experimental purposes, and the parameter values were estimated. It was noticed that the parameters generated from the $k - \epsilon$ model, the mean flow properties, the turbulent kinetic energy, and Reynolds shear stress show good agreement with the experimental data. Although in this paper, the mixing concept wasn't defined, it gave the motivation for future research to consider finer mesh for better estimations.

From Hussain (1986), it can be said that the process of turbulence mixing takes origin from the large structures of the turbulence in the core flow region, giving a clearer

picture of how the turbulence causes the mixing of the fluids into each other. Later, the simulations on the turbulence jets were carried out by Silva et al. (2004) and Akhavan et al. (2000) to determine the properties and energy spectra of turbulent temporal jets.

In the DNS of particle-laden spatial planar jets, it could be inferred that the Stokes number has a non-uniform effect on the spatial distribution of particles. It does have a monotonous effect on the average slip velocity, average particle kinetic energy and the average particle Reynolds number with non-linear scaling laws. The inter-particle relative velocity also takes on a profound dependence on the Stokes number (Kun Luo, 2013). The behavior of a two-way coupling at a very long distance from the entrance behaves the same as that of one-way, but when we compared both behaviors near the nozzle, the centerline velocity decays at a slower rate due to the forcing from the particles (F Picano, 2011).

Simultaneous velocity and concentration measurements can be estimated through experiments of PIV and PLIF and can be compared with the situational results. In the work by Borg (2001), the RANS method for computations is used. The mean profiles that are simulated match well with the experimental result, but there exists the inadequacy of models for the turbulent mass transport based on the standard gradient diffusion concept, which is observed in the experimental data. Differences between the experimental and simulation quantities are found mainly in the cross-sectional plane of concentration fluctuations, for which the experiment data have a lower level. Together with lower values in velocity fluctuations, the turbulent mass transport data estimated through simulation shows a significant difference from experimental data. For better accuracy of the turbulence quantities, a finer model needs to be applied.

The processes of entrainment and mixing in free-shear flows are known to be characterized by a variety of scales ranging from large-scale fluctuations of the turbulent core to small-scale motions acting on convoluted boundaries (A Cimarelli, 2020). The most coherent turbulent structures take the form of quasi-streamwise vortices and high and low streamwise velocity streaks. The topology of these structures is analyzed by their shape and size in the different flow regions of the disorganized motion in turbulent free-shear flows and used to assess the models on turbulent mixing (A Cimarelli, 2022).

In the turbulent planar jet, the shearing motion is stronger than the other motions, but many of the shear layers do not align with the mean shear direction. The enstrophy production in the turbulent planar jet is dominated by the interaction between the motions of shear and elongation. Small-scale shear layers were identified as regions with strong shear. The kinetic energy dissipation in the turbulent planar jet is dominated by the interaction between the motions of shear and elongation in the temporally evolving turbulent planar jets (M. Hayashi, 2021).

A similar study was conducted by Carrasco (2023) in which the droplets were used in place of the particles. The computations are performed using DNS with the liquid phase represented as discrete particles. The physical phenomenon involved is considered to analyze the influence of liquid droplet evaporation & molecular mixing processes described by two distinct multicomponent transport models playing a crucial role in the plane jet development and drastically altering its characteristics before ignition and subsequent combustion stabilization.

1.3 – Current Work

The current work focuses on understanding the scalar transport of the temporal jet in the fluid domain filled with the particles with varying particle characteristics. The simulations are like Masato Hayashi, et al (2021) but instead of passive response of the particles, the active particles are considered to observe the effect of particles in changing the fluid flow. As active particles change the fluid flow and the DNS captures the smallest possible effects based on the Kolmogorov length and time scales, it can estimate how the turbulence parameters such as centerline velocity, Turbulent Kinetic Energy and mixing of the jets are affected due to the particles present in the domain.

The interactions between the particles and fluid are estimated using the Euler – Lagrange approach with no-slip and no-penetration boundary conditions. Also, gravity is ignored due to its low value when compared to that of the fluid velocities. The particle collision is also ignored to reduce the complexity. low particle volume fraction when compared to the fluid volume fraction.

SIMULATION DETAILS

2.1 – Introduction

A range of computational approaches exists for various turbulent multiphase flows based on the Stokes number and particle volume fraction, as shown in Fig 2.1.1. The best approach to solve for the point-particles smaller than the Kolmogorov scale is the Eulerian–Lagrangian point-particle approach (or) Fully resolved approach (S Balachandar, 2010). Some of the common methods of the Eulerian–Lagrangian approach are – (1) Reynolds Averaged Navier-Stokes (RANS), (2) Large Eddy Simulation (LES), and (3) Direct Numerical Simulation (DNS).

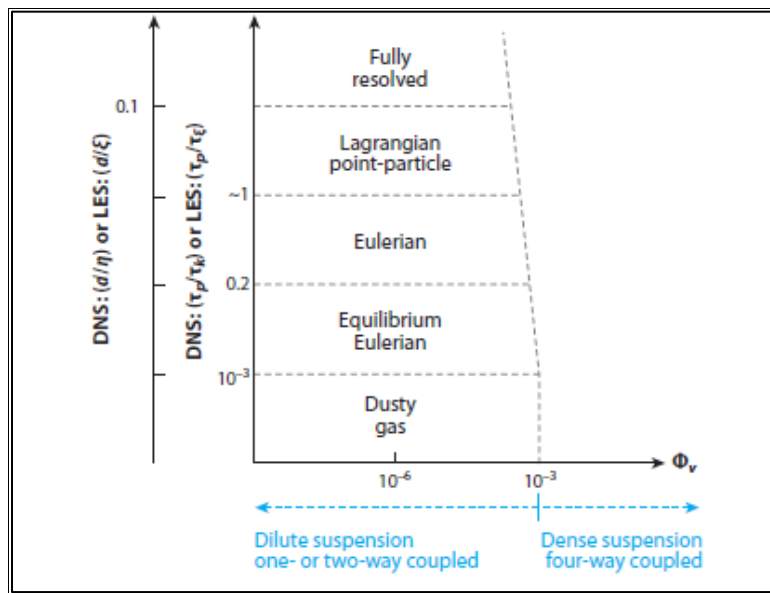


(Fig 2.1.1 – Different approaches to multiphase turbulent flow (S Balachandar, 2010))

The RANS is the turbulent flow approach where the flow quantities are decomposed into their time-averaged and fluctuating components to solve the Navier-Stokes Equations (Durbin, 2001). The LES also solves the Navier-Stokes equation without

approximations but models the smallest length scales. Out of the three, the highest fidelity method to get the resolved physics of the turbulent flows is through the DNS, as it intends to solve the unsteady, three-dimensional Navier-Stokes equation directly without any approximations other than discretization to the smallest length and time scales (Jean M, 2000). Although the DNS solves for the resolved scales, it is computationally expensive due to the comparatively large grid resolutions required in comparison with the other two models. From Fig 2.1.2, it can be inferred that the DNS resolves the flow in all the smallest possible length and time scales. Still, for it to compute successfully, it requires state-of-the-art computational facilities that can provide enough logical processors to simulate the flow within the optimal duration.

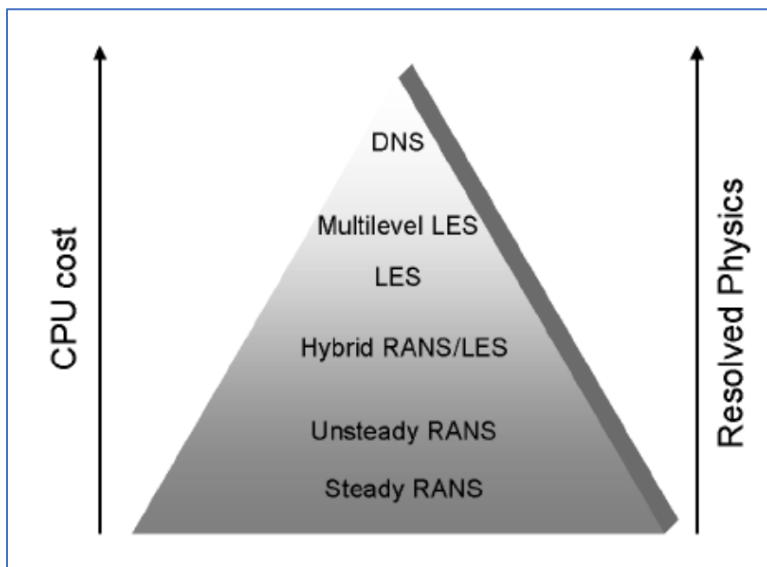


(Fig 2.1.2 – Common methods used in turbulence simulations (Pierre Sagaut, 2013))

Hence in this current work, the simulations are solved using the DNS method. Apart from the DNS method, the point-particle approximation is considered. The main reason for considering the point-particle approximation is that the particle diameter is less than the

grid size. Also, the particle diameter is used to calculate the particle mass density to maintain a constant St. As the particle diameter is less than grid length & isn't used in any of the governing equations, the point-particle approximation is valid for the DNS.

2.2 – Governing Equations

The flow equations that govern the particle-laden turbulent jet flows are the Navier-Stokes equation of incompressible flows for determining the fluid velocity, the scalar transport equation for determining the scalar concentration and the particle transport equation for determining particle location and velocity throughout the domain. As the current work is focused on the fluids at room temperature and low volume fraction of the particles, the temperature component doesn't have any impact on the flow (or) scalar concentration in the domain. Hence it can be ignored in the momentum and transport equations. The two-way coupling is maintained at the particle-fluid interface for the momentum exchange to take place between them. The effective equations for the fluid current work are (Peter J Ireland, 2017):

Continuity Equation:

$$\frac{\partial(1 - \phi)\rho_f}{\partial t} + \nabla \cdot (1 - \phi)\rho_f \vec{u}_f = 0$$

Momentum Equation:

$$\begin{aligned} \frac{\partial(1 - \phi)\rho_f \vec{u}_f}{\partial t} + \nabla \cdot \left((1 - \phi)\rho_f \vec{u}_f \otimes \vec{u}_f \right) \\ = -\nabla p + \mu \nabla^2 \vec{u}_f + \nabla \cdot \mathbf{R}_\mu + (1 - \phi)\rho_f \vec{g} - \overline{F_p^{inter}} \end{aligned}$$

Scalar Transport Equation:

$$\frac{\partial \rho Z}{\partial t} + \nabla \cdot (\rho \vec{u} Z) = \nabla \cdot (\rho D_z \nabla Z)$$

Where ρ_f is the fluid density, \vec{u}_f fluid velocity, ϕ particles volume fraction, p is the pressure, $\overline{F_p^{inter}}$ is the interphase coupling force, \vec{g} is the gravitational acceleration and \mathbf{R}_μ is the tensor that arises from filtering the fluid stress tensor given as $\mathbf{R}_\mu = \mu[(\nabla \vec{u}_f)^T - \frac{2}{3}(\nabla \cdot \vec{u}_f)\mathbf{I}]$, where \mathbf{I} is an identity tensor (Peter J Ireland, 2017) and Z is the scalar concentration and D_z is the diffusivity (O Desjardins, 2013). The particles phase is treated in the Lagrangian frame where every particle is traced. The dynamics of the particles can be calculated using the Newton's second law of motion:

Particles Transport Equation:

$$m_p \frac{\partial \vec{u}_p}{\partial t} = \overline{F_p^{inter}} + \overline{F_p^{col}} + m_p \vec{g}$$

Where \vec{u}_p is the particle velocity, $\overline{F_p^{inter}}$ is the force acting on the particle from Surrounding fluid, $\overline{F_p^{col}}$ is the force due to the collision between the particles. The particles rotation and collision are avoided to reduce the complexity in the simulation. The intercoupling force can be approximated to the drag force due to the uniform flow when the diameter of the particle is less than the flow resolving scale. The drag force can be obtained through many classical models. In the current work the drag model of Tenneti et al. (2011) is employed, that is derived from the particle-resolved DNS. The expression for the drag is given as:

$$\frac{f_i^{drag}}{m_p} = \frac{1}{\tau_p} (u_{f,avg} - u_p) F(\varepsilon_f, Re_p)$$

where τ_p is the particle response time, $F(:, :)$ is the dimensionless drag force coefficient, ε_f is localized volume fraction of the fluid and Re_p is the particle Reynolds number. The final expression for the dimensionless drag coefficient is as follows:

$$F(\varepsilon_f, Re_p) = \frac{(1 + 0.15Re_p^{0.687})}{\varepsilon_f^2} + \varepsilon_f F_1(\varepsilon_f) + \varepsilon_f F_2(\varepsilon_f, Re_p)$$

$$Re_p = \frac{\varepsilon_f \rho_f |u_f - u_p| d_p}{\mu}; F_1(\varepsilon_f) = \frac{5.81(1 - \varepsilon_f)}{\varepsilon_f^3} + \frac{0.48(1 - \varepsilon_f)^{\frac{1}{3}}}{\varepsilon_f^4};$$

$$F_2(\varepsilon_f, Re_p) = (1 - \varepsilon_f)^3 Re_p \left(0.95 + \frac{0.61(1 - \varepsilon_f)^3}{\varepsilon_f^2} \right)$$

In this current work, the above defined equations are used for solving the particle-laden jet simulations. The simulations are non-dimensionalised before solving the equations. The spatial non-dimensionalisation is done through the jet slot width, $h = 1$. The time and the mass non-dimensionalisation are done through the fluid viscosity and density respectively ($\mu_f, \rho_f = 1$).

There are many dimensionless quantities that characteristic properties of the fluid flow. In this current work, some of the commonly used dimensionless quantities that are used in the simulation calculations are Reynolds Number (Re_f), Schmidt Number (Sc_f) and Stokes Number (St). Reynolds number is defined as the ratio between the inertial and viscous forces. Schmidt number is defined as ratio of the momentum diffusivity to the mass

diffusivity. Stokes Number is defined as the ratio of characteristic time of the particle to the characteristic time to flow. Based on the above definitions, equating them into the fundamental fluid and the particle-related properties with non-dimensionalisation ($h, \mu_f, \rho_f = 1$) leads to:

$$\text{Reynolds Number, } Re_f = u_{jet};$$

$$\text{Schmidt Number, } Sc_f = 1;$$

$$\text{Stokes Number, } St = \frac{\left(\frac{\rho_p d_p^2}{18}\right)}{t_d}.$$

Where u_{jet} is the velocity of the jet, ρ_p is the density of the particles, d_p is the diameter of the particles, t_d is the fluid response time which is the Kolmogorov time scale.

2.3 – Solver Algorithm

For the current work, the NGA solver developed by O Desjardins and G Blanquart (2005) runs the DNS simulations. NGA solve is one of the efficient and capable software used to solve LES and DNS simulations for low-Mach number Navier-Stokes, Scalar and particle transport equations on structured meshes. The numerical methods used in the NGA can be implemented in parallel computational mode using message passing interface (MPI) significantly reducing the simulation time (J Capecelatro, 2013). The solver uses stagnation meshing for the velocities to avoid the problem with aliasing. Also, during the recent times, it is noticed that the second order finite difference schemes on the stagnation meshes conserves the kinetic energy discretely ensuring its robustness along with a good method

to simulate the turbulence (Harlow and Welch, 1965). The discretizational schemes for solving the equations used in the NGA solver are proposed by O Desjardins (2008 & 2013).

The flow of the NGA solver is as follows. Initially, the momentum equation is predicted by using the Adam-Bashforth method in determining the pre-final velocity of the fluid. The predicted fluid velocity is calculated to determine the final particle positions and velocities by solving the particle transport equation using the second-order Runge-Kutta scheme. Once the particle parameters are estimated, drag model formulation is used in estimating the interphase terms along with the finalized volume fraction and density in all the grids. The next parameters that are solved are the Scalars. In the current work, the scalars that are estimated is only the scalar concentration evaluated in-terms of mixture fraction. This scalar is solved from the scalar transport equation using third order WENO scheme due to the high stability of the computational models (J Capecelatro, 2013). Finally, the velocity of the fluid is accurately computed by using the second-order Crank-Nicolson scheme for overall momentum equations. The above process is applied for the simulation in which the pressure gradient is very low. For significant pressure gradient, the fluid velocities are recomputed at the boundary or the edges by solving the continuity equation, that is transformed as the Poisson equation (O Desjardins, 2008). The pressure Poisson equation is solved using the combination of energy spectral, Krylov and multi-grid-based method as proposed by Y Morinishi, et al. (1998) to enforce the continuity condition. This cycle flow is repeated by advancing the time step, till the time reaches the target value.

2.4 – Meshing & Grid Parameters

For smaller Reynolds numbers the viscous forces are more significant than the advection forces. As a result, the flow fluctuations are gradually reduced making the turbulence to eventually die down over time. Whereas for large Reynolds numbers, the advection forces are greater in magnitude relative to the viscous force, resulting in the laminar (or) jet flow instability. As these flow instabilities grow larger, continuous generation of turbulence occurs. This generation produces the large-scale eddies, which are in-turn unstable and break down and cause smaller eddies. This cascading process goes on till the scale at which the viscosity is stronger enough to hold the fluid from causes further breakup of eddies. This smallest scale under which the breakup of eddies mostly doesn't occur is called the Kolmogorov scale (Davidson, 2004).

This Kolmogorov scale has 2 components – (1) Kolmogorov length scale and (2) Kolmogorov time scale. Both scales estimates vary with the turbulent flows and their dimensionality of the shear propagation as they relate to the turbulent kinetic energy dissipation rate. The general equations of these scales are: (SB Pope, 2000)

$$\text{Kolmogorov length scale, } \eta_d \sim \left(\frac{v^3}{\epsilon} \right)^{\frac{1}{4}} ; \text{Kolmogorov time scale, } t_d \sim \left(\frac{v}{\epsilon} \right)^{\frac{1}{2}}$$

For the turbulent jets, the estimates for Kolmogorov length scales were generated in the past by (Antonia, 1979) are as follows, which need to be resolved by the discretization for DNS implementations:

$$\text{round jets : } \frac{\eta}{d} = (48Re_f^3)^{-\frac{1}{4}} \left(\frac{x}{d}\right); \text{ planar jets : } \frac{\eta}{d} = 0.94 Re_f^{-\frac{3}{4}} \left(\frac{x}{d}\right)^{\frac{5}{8}}$$

2.5 – Initial & Boundary Conditions

For the initial condition in temporal jets, the jet propagation direction is filled with the jet flow & its velocity in the jet width domain which can be written as:

$$u = u_{jet} * (1 + n (R\{0,1\} - 0.5)), |y| < \left(\frac{h}{2}\right)$$

This helps in generation of uniform jet velocity throughout the jet width in the propagation direction. Noise, n is also added so that the jet attains the turbulent state faster than the non-noise case by faster build-up of the eddies due to velocity gradients of the jet with the surroundings. Coming to the boundary conditions, the entire domain is taken as the periodic in three directions i.e., mass exiting out with certain velocity enters the domain again with the same speed on the opposite end.

SIMULATION INPUTS

From BK Reville (1992), a jet will be laminar if $Re_f < 100$ and it will be turbulent if $Re_f > 2000$. Also, a turbulent jet flow can be divided into two distinct regions – (1) flow development region, and (2) fully developed region. The flow development region is inversely proportional to the Re_f . This implies that the smaller domains can be considered for the larger Re_f . So, for this work the uniform temporal slot jet with $Re_f = 5000$ coming out from slot width of h with particles at rest and domain dimensions of $10h \times 5h \times 2.5h$ is considered for the simulation. The jet velocity has a 10% noise component added on top of the mean value.

To understand the turbulence phenomenon and capture the smallest eddies possible, the grid size is estimated based on the Kolmogorov length and time scales. It is considered at 95% of Kolmogorov scale at $10h$ and at the initial velocity conditions of one eddy turnover times implying its effective value to be $6.60e-03$. This grid scale causes the domain to be divided into $1516 \times 758 \times 379$ uniform grids in each direction. The time step is maintained in such a way that it is less than the minimum of Kolmogorov time scale and the eddy turnover time ($t_e = \frac{h}{u_f}$) to capture the smallest eddies possible during the simulation. The minimum eddy turnover time and the Kolmogorov time scale turns out to be $1.32e-06$ and hence the timestep of $1.25e-06$ is considered for all the different cases of the simulations to capture the smallest eddies possible. The simulations are run till $60t_e$, to understand the decay of the scalar concentration and velocity of the jet to the fluid domain filled with particles of different configurations in each case.

The particles are allocated in the domain of $9.8h \times 4.8h \times 2.3h$, giving clearance of $0.1h$ from the domain faces to prevent the solution blow-up during the start. The two-way coupling is used in the simulation to understand the effect of particles on the jet.

This set of same configurations is considered for 4 cases of different St by changing the particle density. The particle diameter is taken as half of the grid size. Also, the particles volume fraction is changed such that the effective particles mass to the fluid mass will be unity (i.e., mass fraction, $\phi_m = 1$). Based on the above set of inputs, the configurations for the different DNS cases are shown in the below table:

Sim No	Stokes No	Particles Diameter	Particles Density	Particle Vol. Frac.	Particle Mass Frac.	No. of Particles
1	0	-	-	-	-	0
2	1	3.30e-03	74	1.60e-02	1	~91.42 million
3	7.5	3.30e-03	555	2.25e-03	1	~12.85 million
4	20	3.30e-03	1480	7.85e-04	1	~4.45 million

(Table 3.6.1 – Configurations of the DNS simulations for different St)

Each of the above-mentioned simulations had requested 512 CPU cores of high computational performance. These nodes are typically called parallel nodes in the Agave cluster and are with the configuration of Intel® Xeon® Processor E5-2680 v4. To achieve the results up to $60t_e$, the simulations are run approximately for 5 days.

RESULTS & DISCUSSIONS

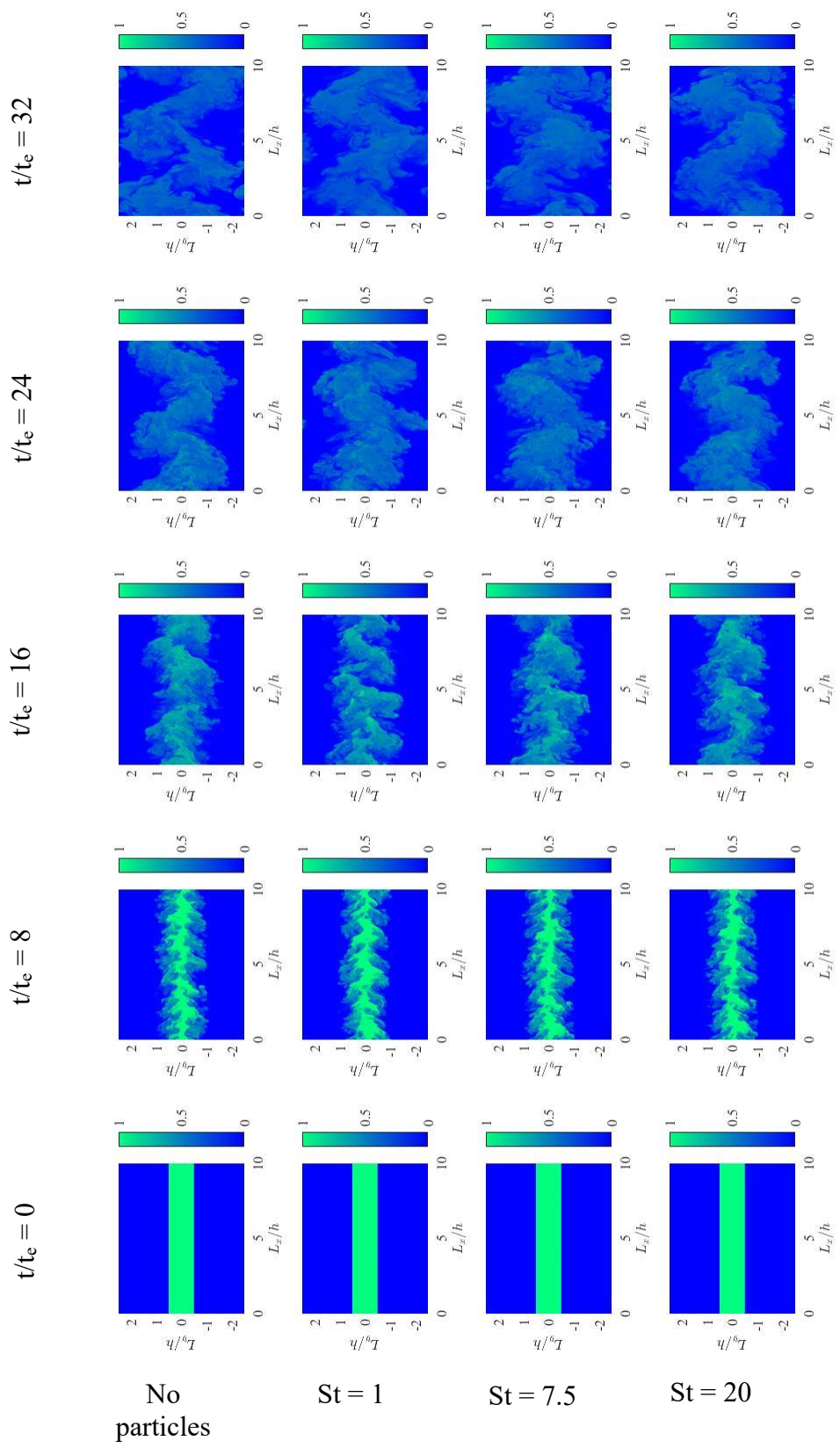
4.1 – Simulation Analysis

The approaches used are – (1) qualitative analysis and (2) statistical analysis. In qualitative analysis, the cross-stream flows of different St are compared with each other at different eddy turnover times (t_e). The other analysis carried out is statistical analysis. The statistical analysis is carried out in 2 planes – (1) streamwise – normal ($x - y$) plane, and (2) streamwise – parallel ($x - z$) plane. Although 193 datasets were generated when the simulations for each case ran for $60t_e$, the analysis is capped to $35t_e$, corresponding to 112 datasets for better analysis and comparison of turbulence with different St , without considering the impact of periodic boundary conditions.

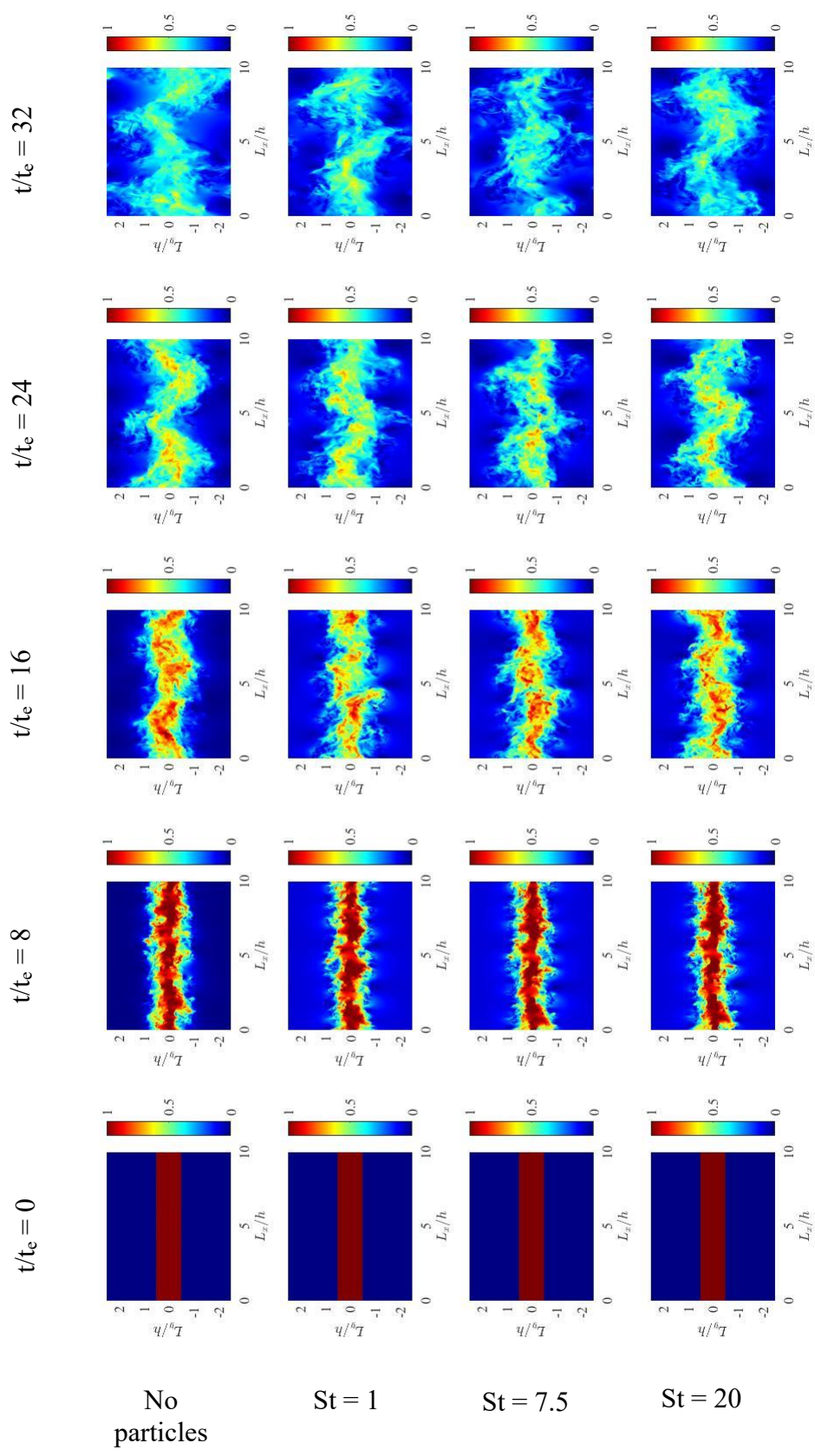
4.2 – Qualitative Analysis in Streamwise-Normal Plane

The streamwise-normal plane is considered for the qualitative differentiation and analysis of different St cases. The slice of $0.01h$ is considered for the analysis which is a good representation of the particle and fluid properties in two dimensions. The scalar and the velocity plots in the streamwise-normal plane at various times ($0t_e, 8t_e, 16t_e, 24t_e, 32t_e$) for all the St (0, 1, 7.5, 20) are in Fig 4.2.1 & 4.2.2 respectively.

From Fig 4.2.1 & 4.2.2, the jet spreading in cross-plane direction was comparatively less for higher St . This is due to particles acting as the obstruction for the jet to expand in cross-plane direction. Due to the jet velocity in cross-plane direction to be low, the particles in higher St provide higher resistance and further reduce the cross-stream jet velocity eventually reducing the spread of jet in streamwise-normal direction.



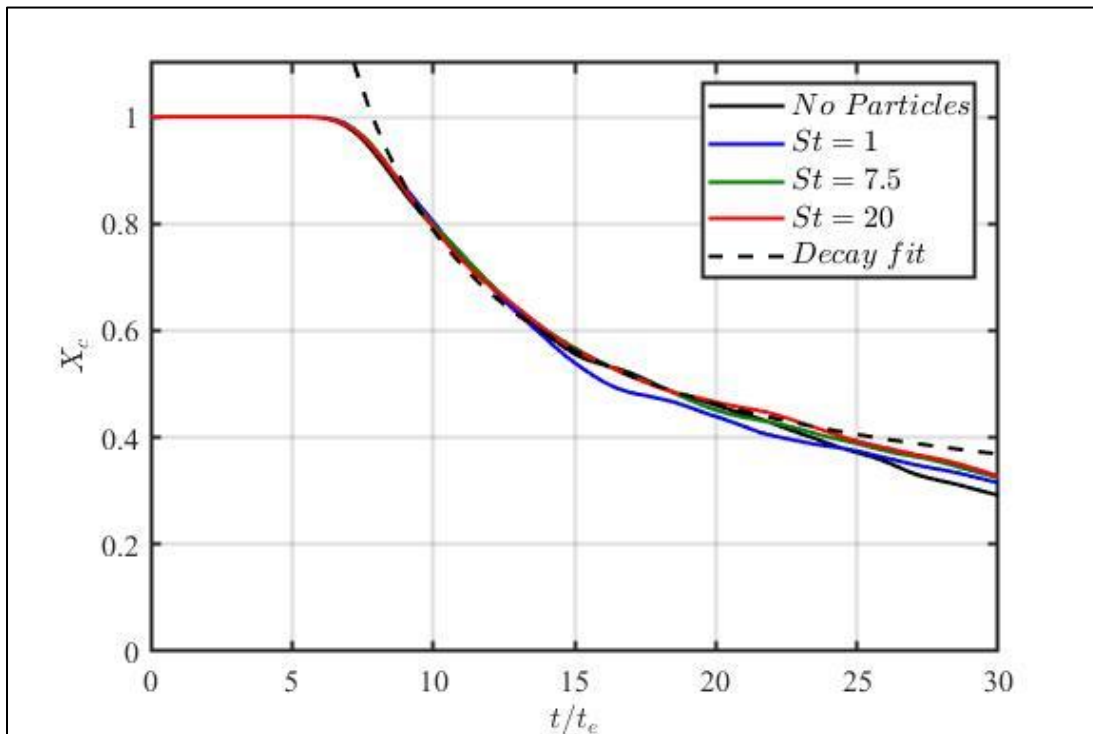
(Fig 4.2.1 – Jet mixture fraction profiles in span-wise direction for different St (top-bottom) at different t_e (left-right))



(Fig 4.2.2 — Jet velocity profiles in span-wise direction for different St (top-bottom) at different t_e (left-right))

4.3 – Statistical Analysis in Streamwise-Parallel Plane

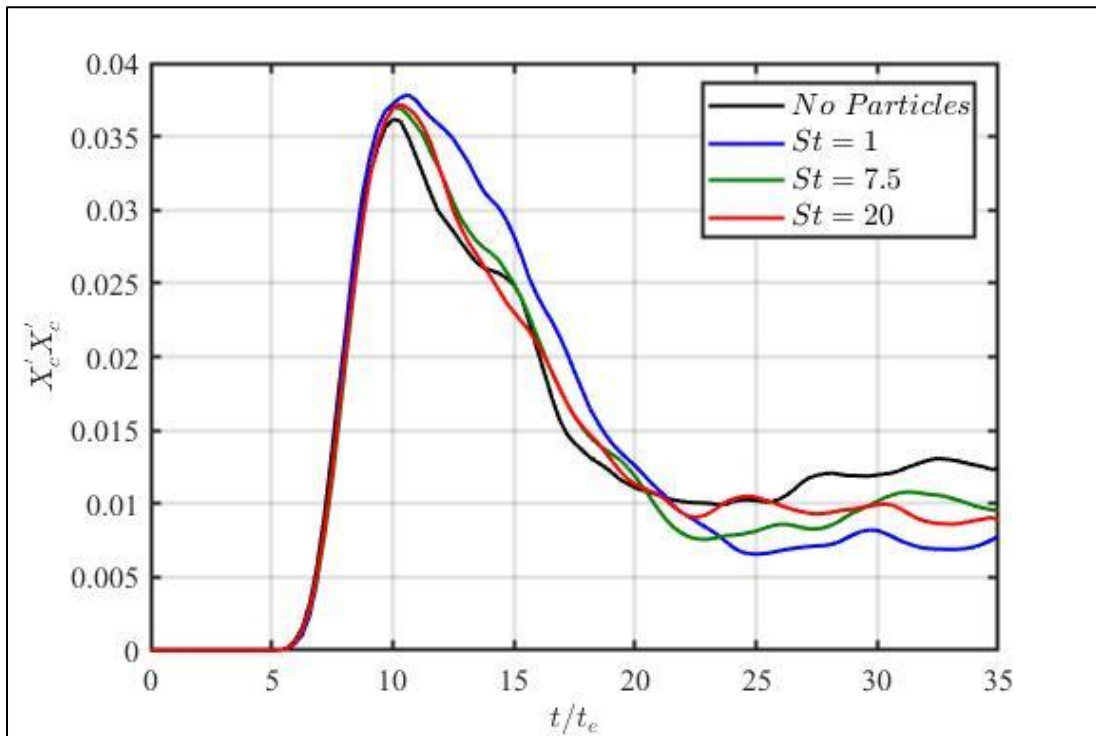
The centerline data ($y=0$) is considered for further analysis of the fluid and particles flow. The mean statistics for the mixture fraction of the jet is shown in Fig 4.3.1. There is no significant difference in the mean mixture fraction decay over time for different St . The theoretical final value of the mixture fraction decay over long t_e time can be computed as 0.2. From figure 4.3.1, evidence of decay approaching the value of 0.2 for the long stable t_e . When the decay data is fit to the exponential curve fitting of the form $y - y_0 = \frac{a}{x-x_0}$, the virtual origin for the decay is $\sim 2.02t_e$.



(Fig 4.3.1 – Mean of Mixture fraction over time for various St)

Unlike mean, the variance yields distinct difference between various St . The variance plots for the mixture fraction of the jet for different St are shown in Fig 4.3.2. The

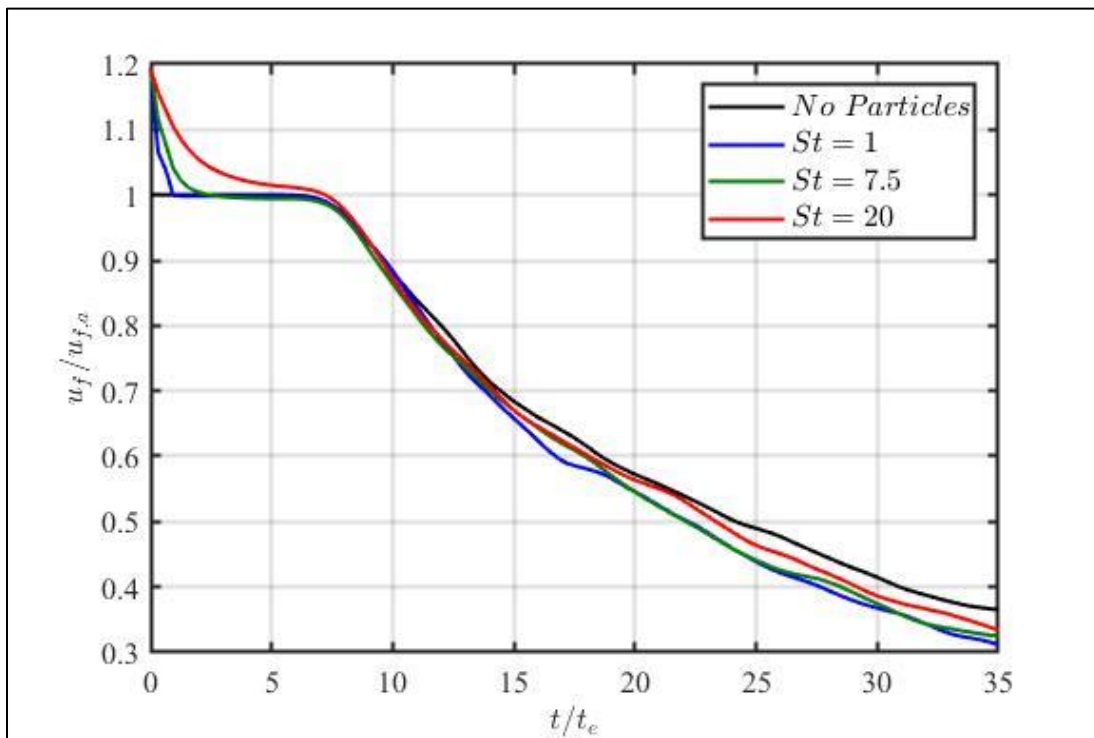
maximum variance in the scalar mixture fraction is noticed at time $\sim 10t_e$. Beyond that time, the variance decreases and converges to a value. Also, it can be observed that variance of $St = 0$ is low and then is increased till $St = 1$ and then decreased for the remaining higher order St . This could be inferred that the scalar mixture fraction variance increases till $St = 1$, compared to the particle-free and higher St , indicating that an optimal St exists for which the scalar variation is maximum. Here, the variance isn't converging due to the finite domain effects.



(Fig 4.3.2 – Variance of Mixture fraction over time for various St)

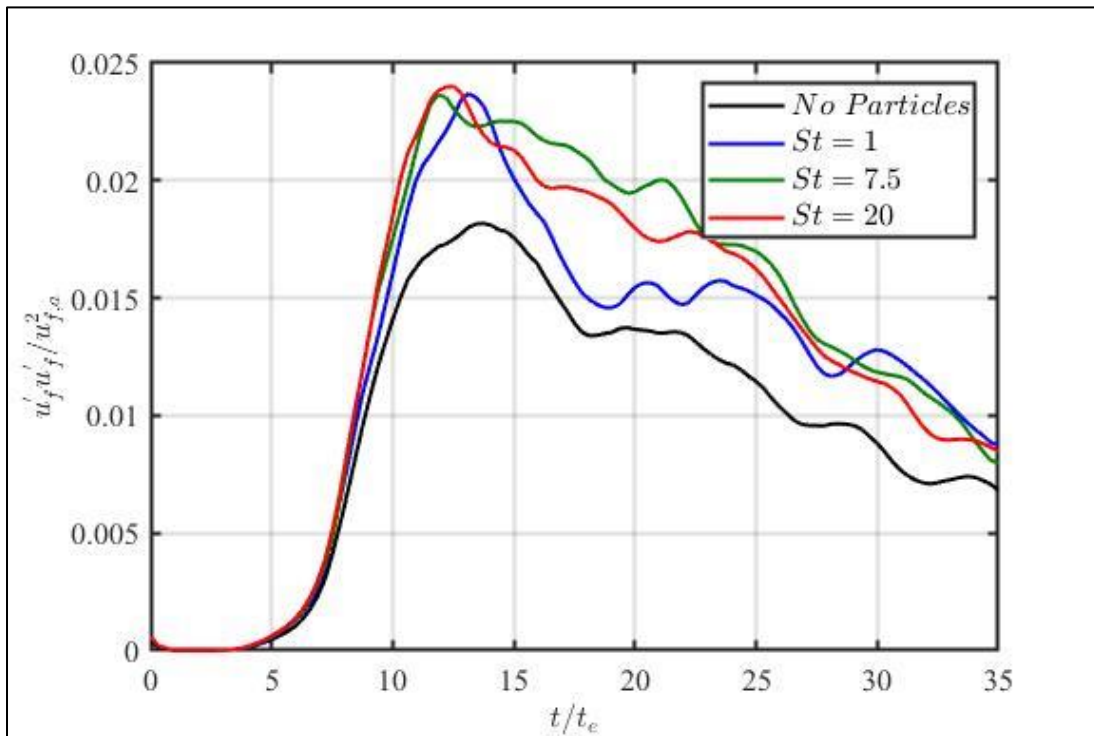
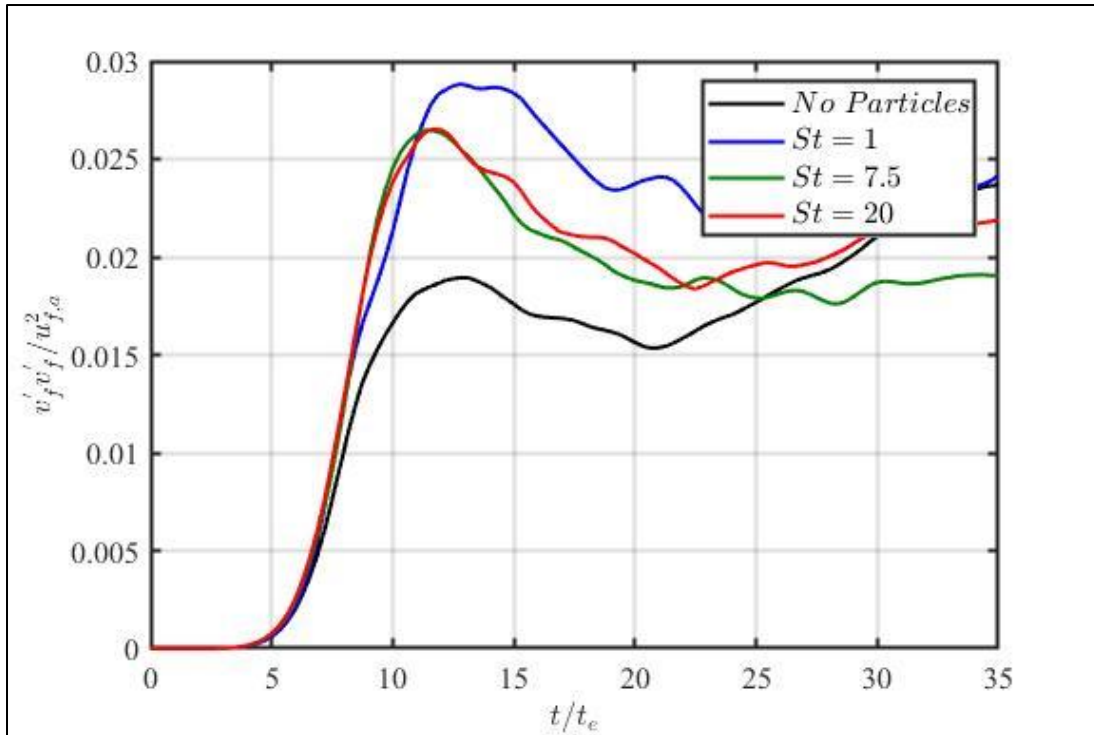
The streamwise jet velocities (u_f) for different St are analyzed and plotted in figure 4.3.3. All cases are initialized at the same fluid velocity. However, the particles are initialized at rest, and thus momentum transfer occurs between the fluid and particle media.

This results in an observable shift during the start for particle-laden jets in comparison with particle-free jet. The asymptotic velocity of the fluid medium after reaching the equilibrium with particle state is referred henceforth as called asymptotic jet velocity ($u_{f,a}$) for each St , which is used to normalize the velocities. Just like in the scalar concentration case, no significant difference for the jet mean streamwise velocity (u_f) for different St over time are observed at the centerline.



(Fig 4.3.3 – Spanwise velocities of the jet fluid for various St)

The plots for the variance for the jet velocity, u'^2 , v'^2 and w'^2 in each direction are given in Fig 4.3.4. The turbulence kinetic energy (TKE_f) is plotted based on the values of self-variance and is plotted in Fig 4.3.5.



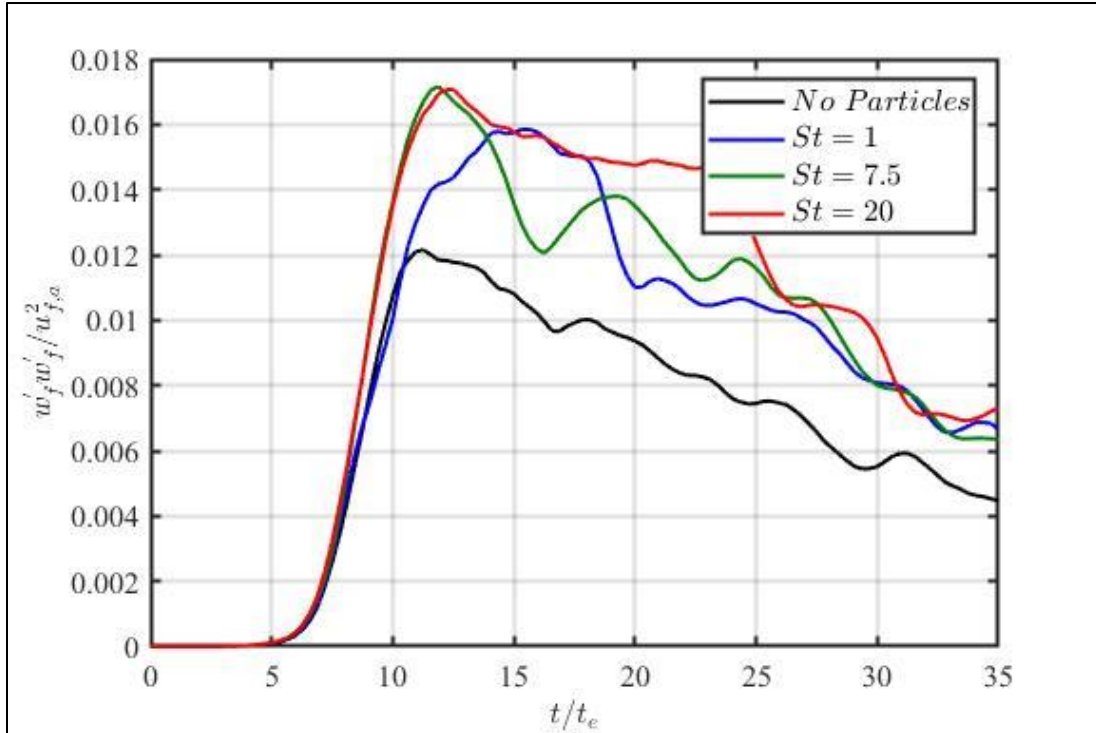


(Fig 4.3.4 – Variance of the jet velocity in (a) Streamwise, (b) Cross-stream, and (c) Spanwise directions, for various St over time)

From Fig 4.3.4, the particle-free case shows significantly different signs in comparison with the different particle-laden cases. The particle-free flow is significantly less due to the reason that the asymptotic velocity of the particle-free case is more when compared to that of the particle-laden case. This makes the denominator of the non-dimensionalised variances and TKE to be significantly more leading to their overall lesser value. In most of the conditions, the peak is observed at $\sim 12t_e$, beyond which the variance values tend to converge just like in the case of scalar mixture fraction.

From Fig 4.3.5, the TKE_f peak is observed comparatively at later time for $St = 1$ in-comparison with the other St . Also, the TKE_f is significantly more for $St = 1$ than

other implying that the optimal value occurs at $St = 1$ rather than at lower & higher St . But there isn't significant difference between different St after certain time. This implies that after certain time, the TKE_f profiles would be same. The TKE_f converges to the value of $0.02u_{f,a}^2$ and begins to converge once time goes beyond $12t_e$.

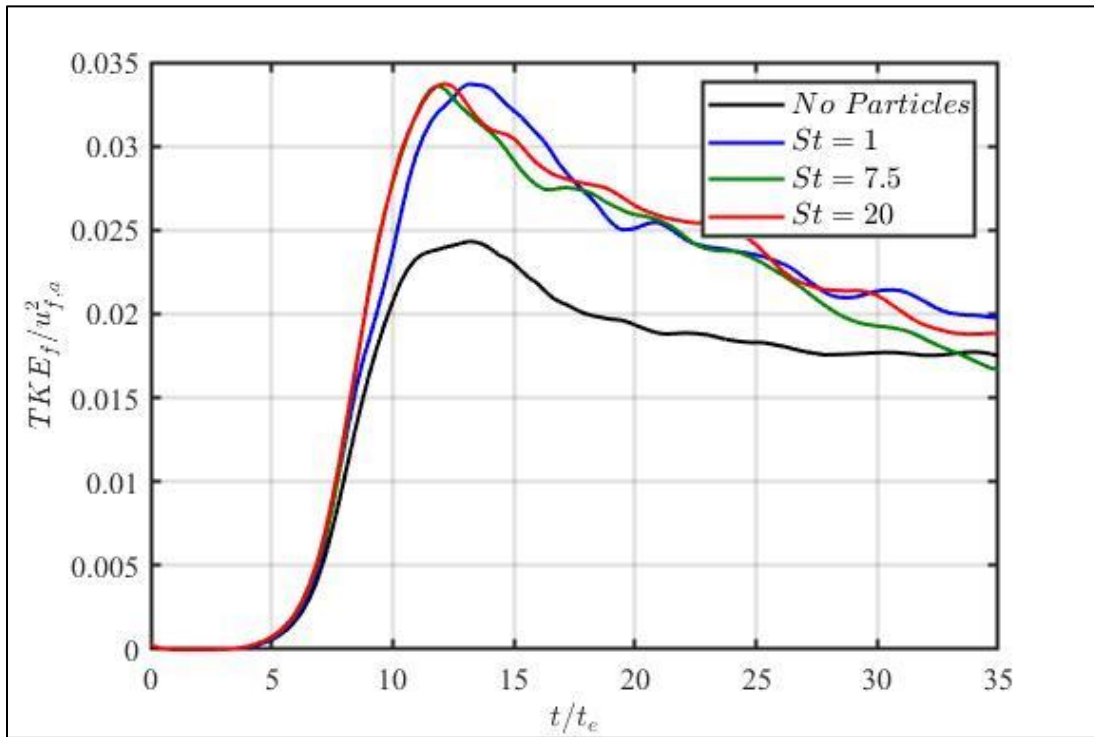


(Fig 4.3.5 – Turbulent Kinetic Energy of the jet (TKE_f) for various St over time)

The particles spanwise velocities are analyzed and are plotted in Figure 4.3.6 and is observed that the velocities of the particles for $St = 1$ case attains the jet velocity faster than the $St = 20$ case. Although it attains velocity faster, it also loses velocity faster in comparison with that of the latter case. Ultimately the particle velocities converge to the same value as that of the final jet velocity after long times ($t \sim 35t_e$).

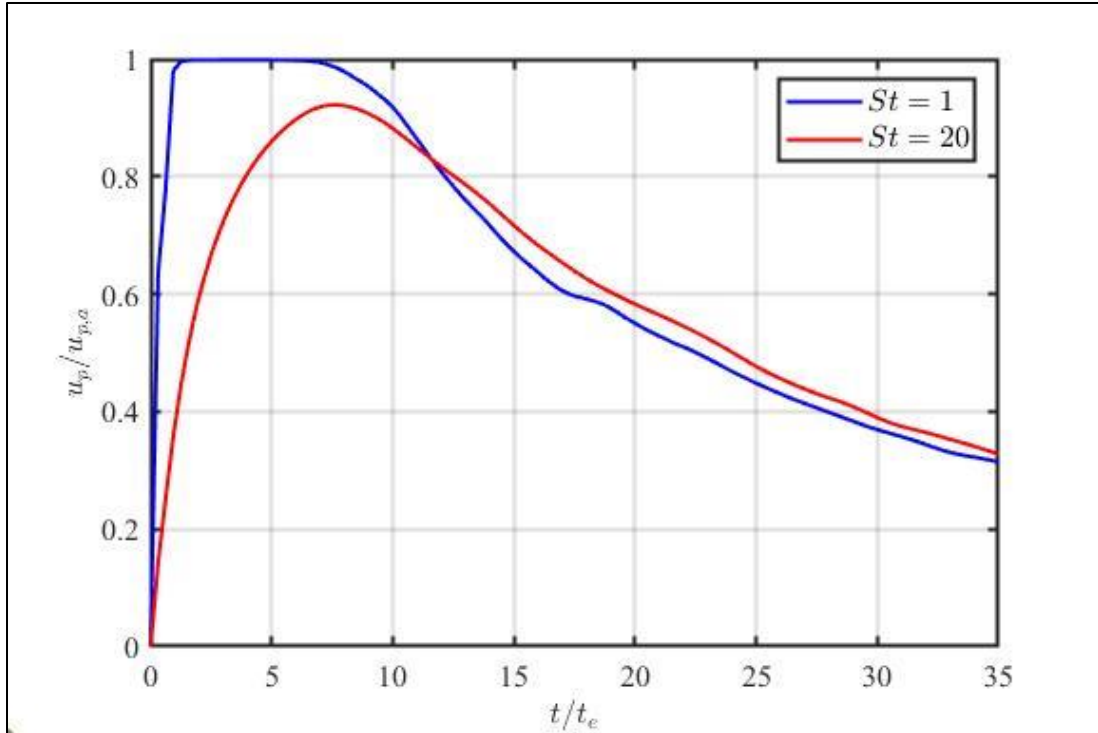
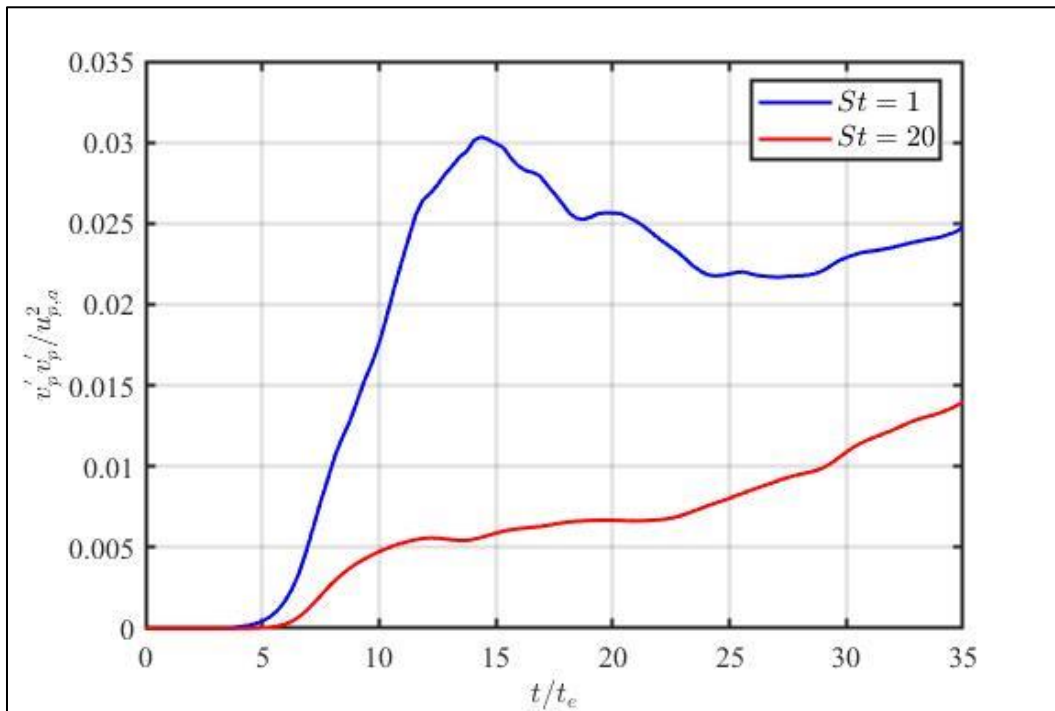
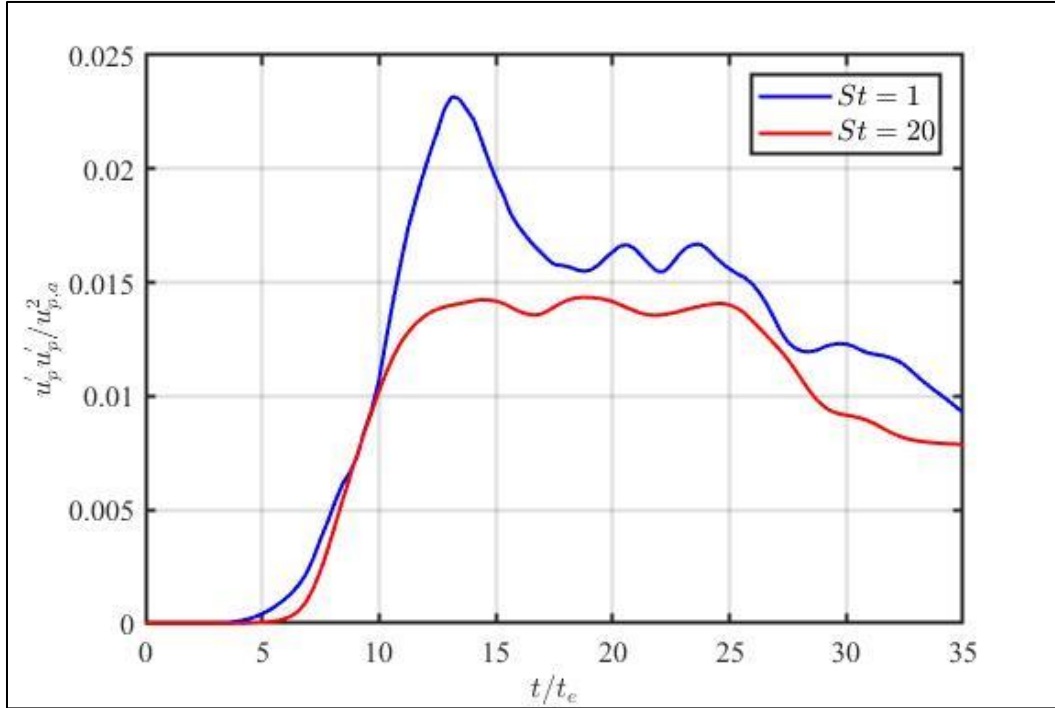


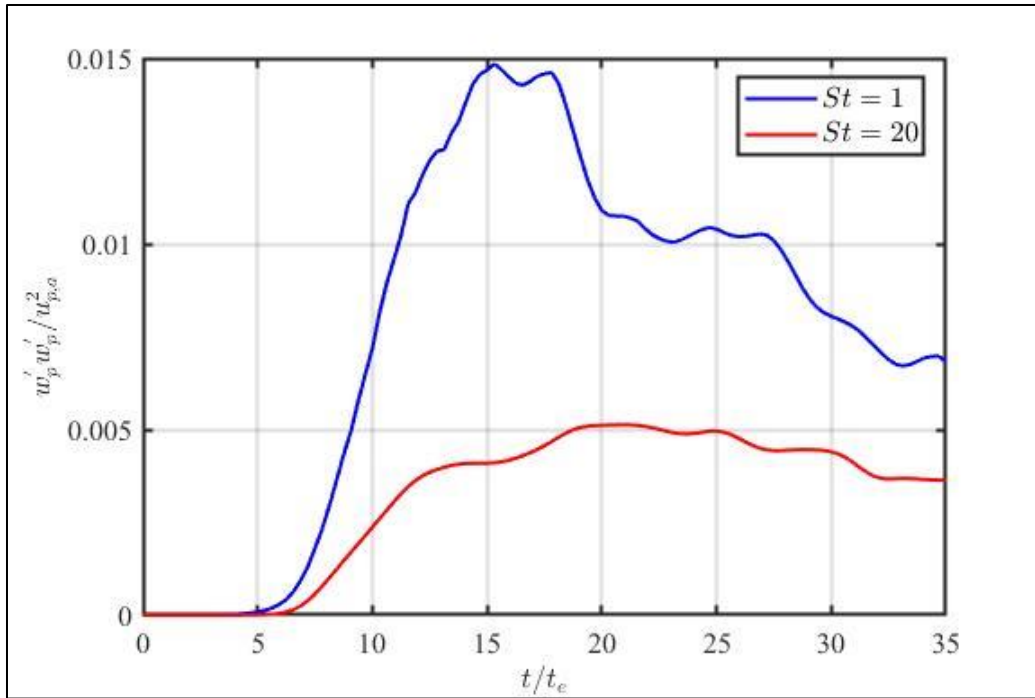
(Fig 4.3.6 – Spanwise velocities of the particles for various St over time)

The plots for the variance for the particle in each direction are given in Fig 4.3.7. The turbulence kinetic energy for the particles (TKE_p) is plotted based on the values of self-variance and is plotted in Fig 4.3.8.

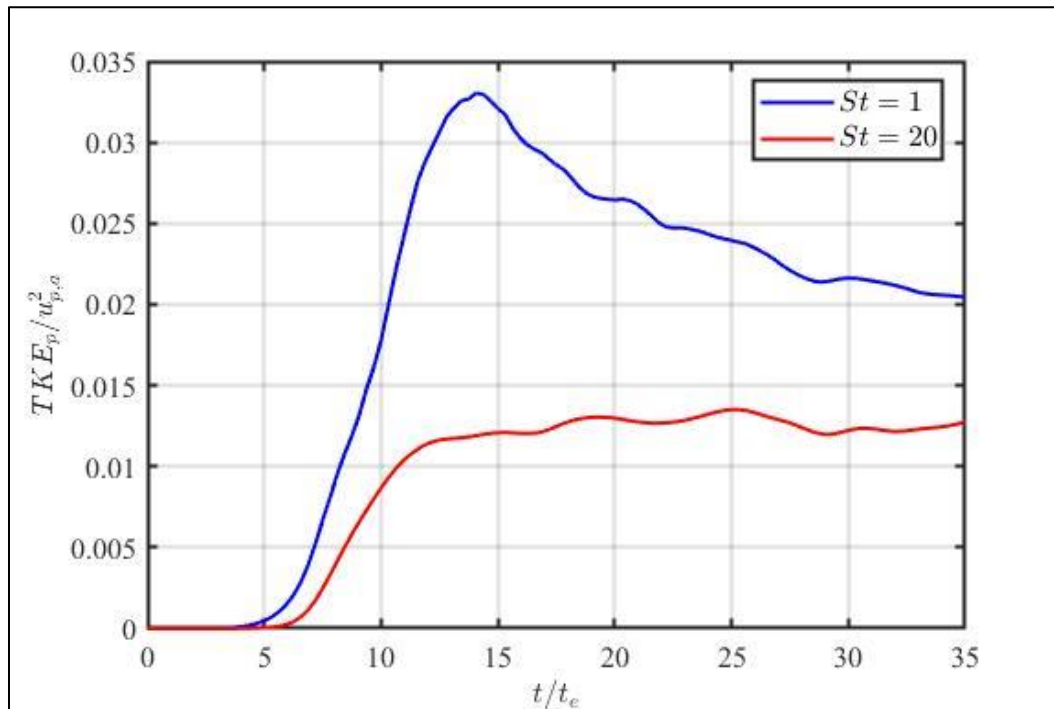
From Fig 4.3.8 irrespective of the velocity direction, the larger St TKE_p is less when compared to the smaller St one. This same is reflected in the TKE_p plot as it is the sum of the variance in all the directions. From the TKE_p plot in Fig 4.3.8, the transfer of energy in-between the fluid and particles for lower Stokes number is significantly faster when compared to that of the larger ones. This implies that the peak is attained quickly and closer to the time when the TKE_f peak attains maximum value. It also indicates that it can

freely absorb and give away energy to the fluid domain. For larger St , the peak might not be noticed as it takes huge particle response time for the energy to transfer from fluid.





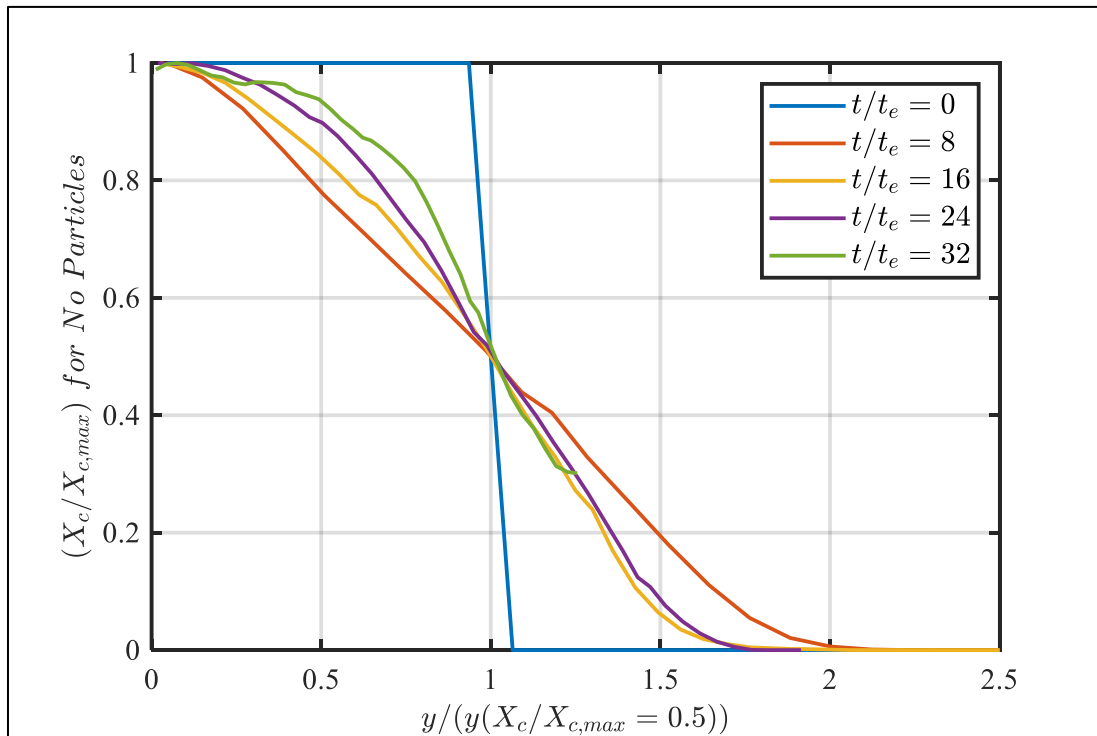
(Fig 4.3.7 – Variance of the particle velocity in (a) Streamwise, (b) Cross-stream, and (c) Spanwise directions, for different St over time)

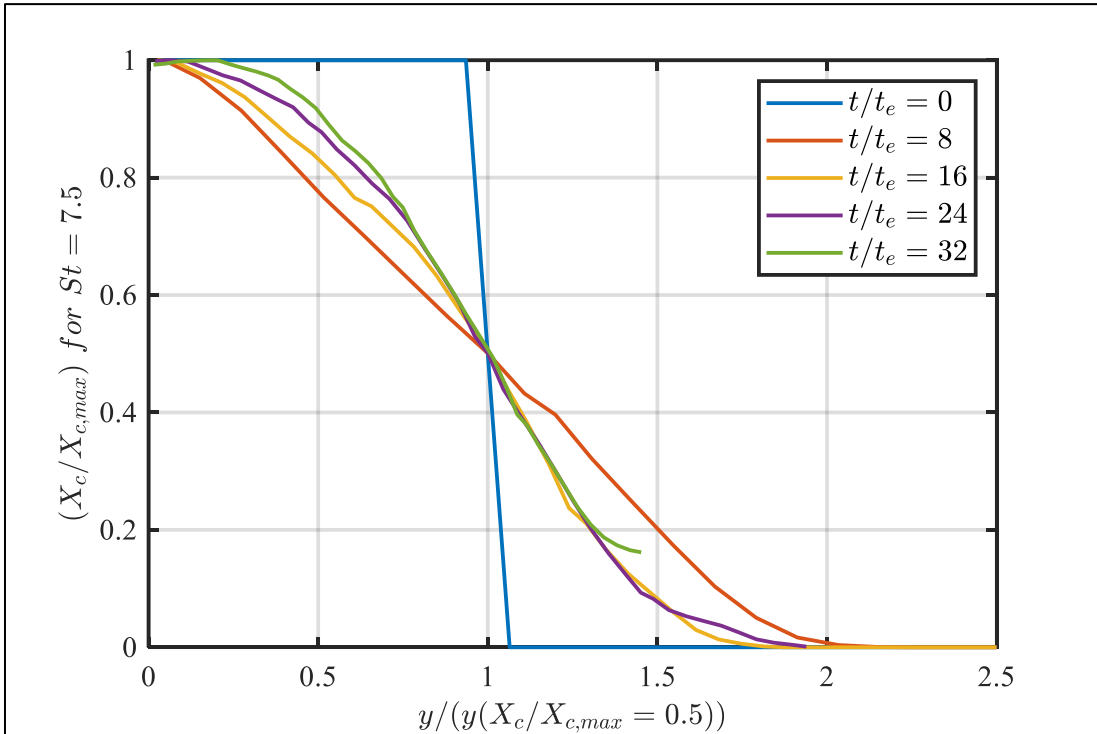
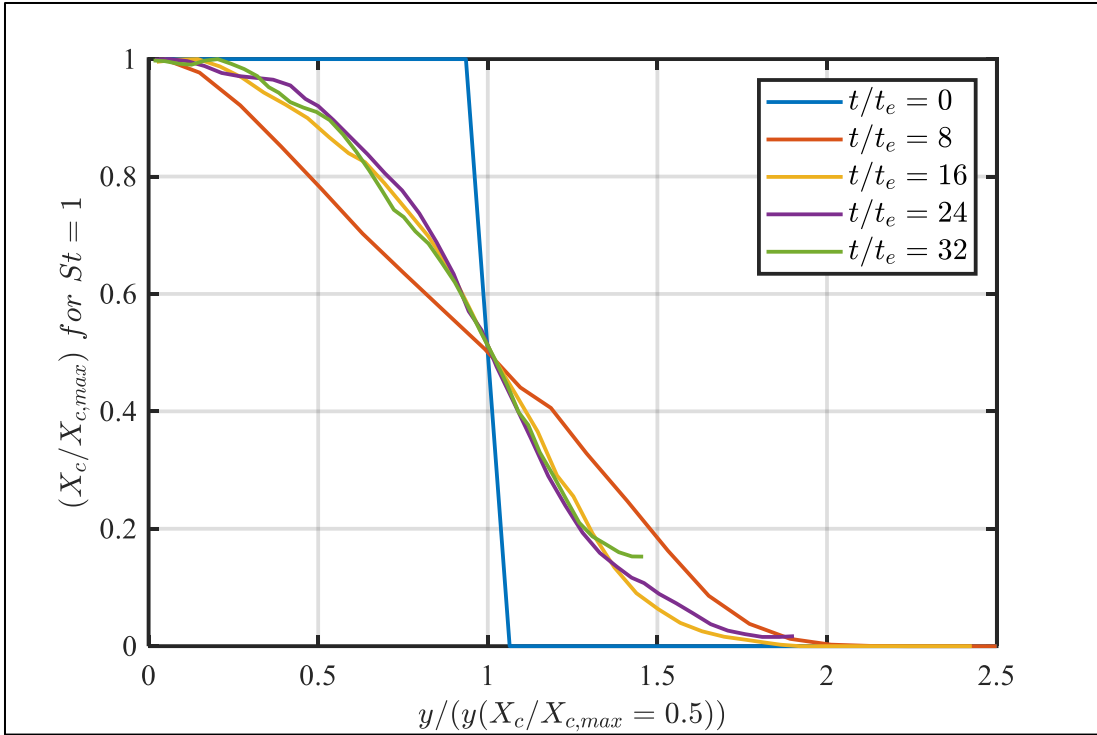


(Fig 4.3.8 – Turbulent Kinetic Energy of particles (TKE_p) for various St over time)

4.4 – Statistical Analysis in Streamwise-Normal Plane

Like the streamwise-parallel plane analysis, the mean and the variance statistics of various fluid and particles properties are analyzed for the re-constructed streamwise-normal data ($z=0$) for deeper understanding of the fluid and particles flow. Here, the half-width profiles are considered due to the symmetry in the cross-stream. The mean statistics for the mixture fraction of the jet in the cross-stream direction St is shown in the Fig 4.4.1.





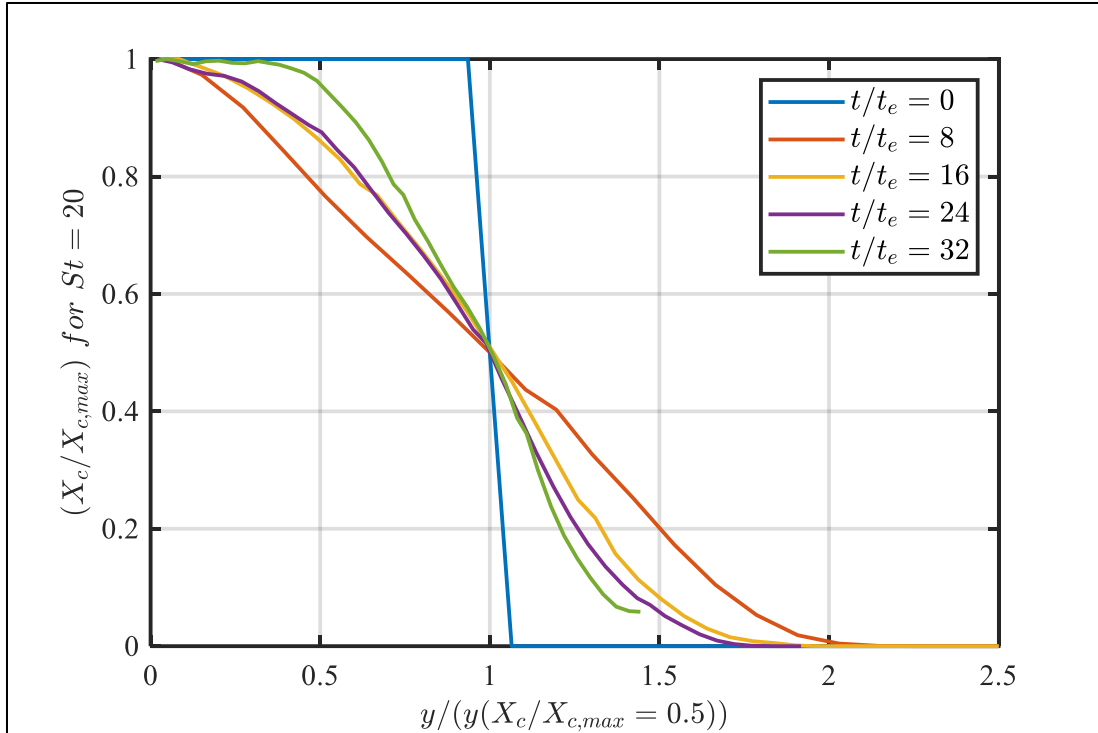
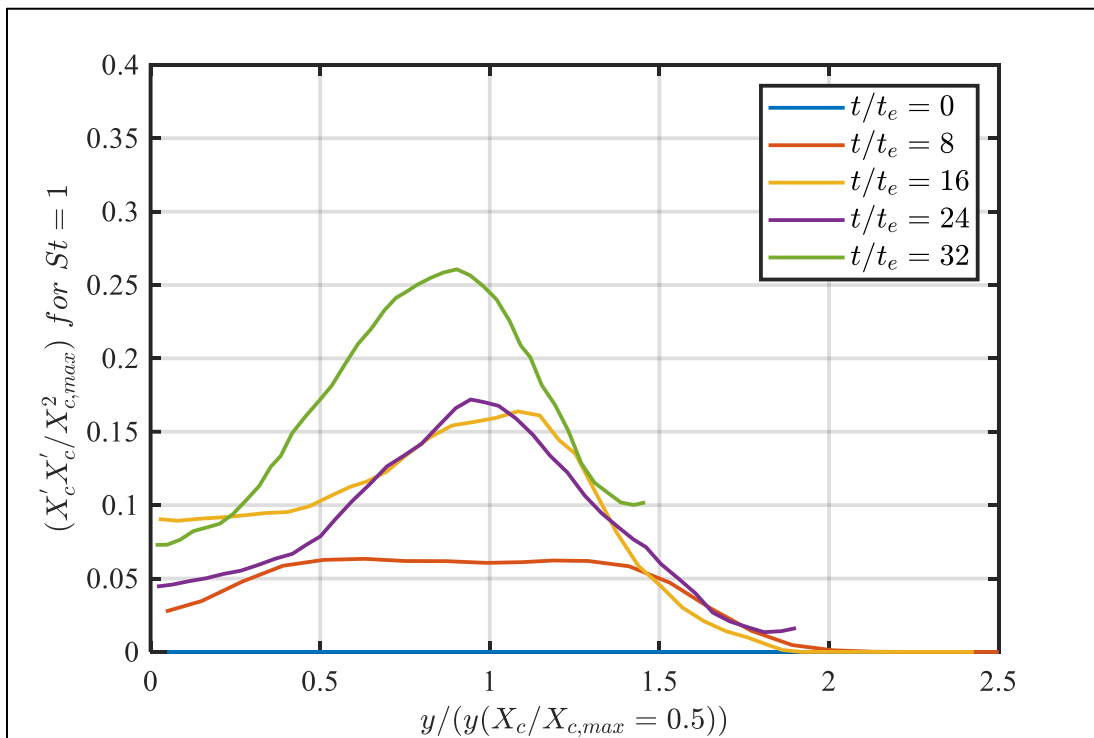
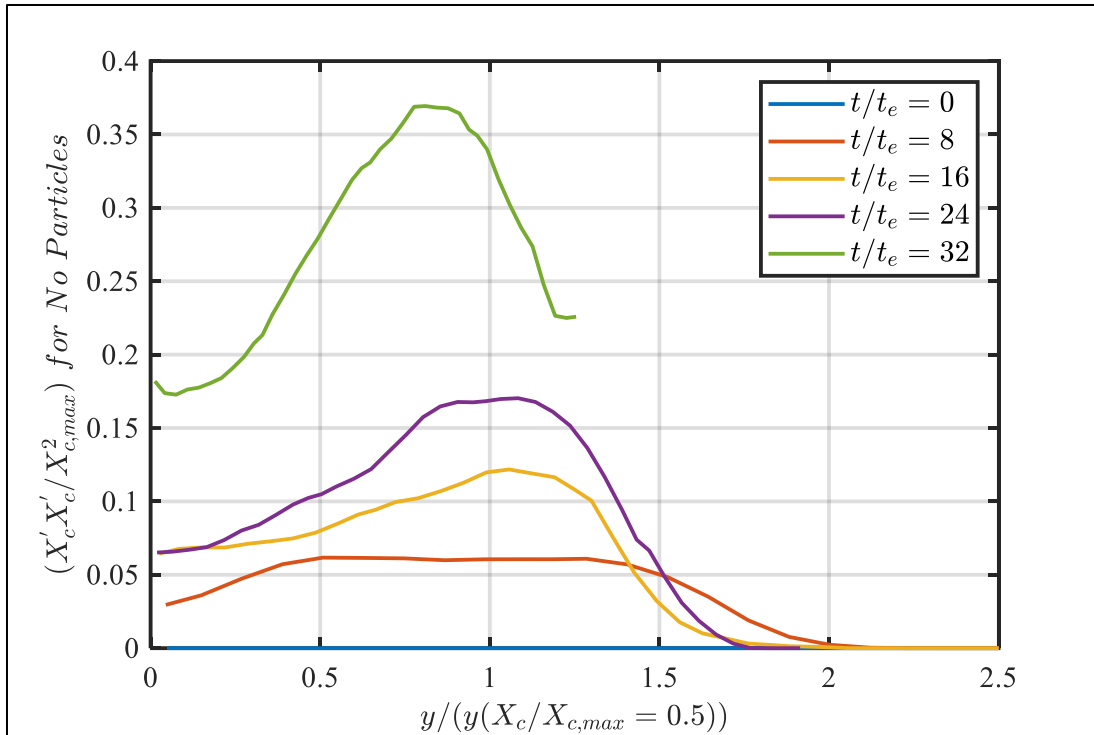


(Fig 4.4.1 – Mean of Mixture fraction over time for

(a) No Particles, (b) $St = 1$, (c) $St = 7.5$ and (d) $St = 20$)

Initially for the lower t_e , no significant difference between various St are observed. As the t_e increases, the difference between the profiles of mixture fraction grows and becomes significance among themselves and the other St cases. Although the differences start to grow, the maximum value is always achieved at the center of the jet half-width irrespective of St . From the Fig 4.4.1, the mixture fraction spread along the cross-stream decreases with increase in the St .

Unlike the mean statistics of the mixture fraction where the mean stays at the center of the cross-stream width, the variance yields a difference result. These variance plots along the jet cross-stream half width for different St are shown in Fig 4.4.2.



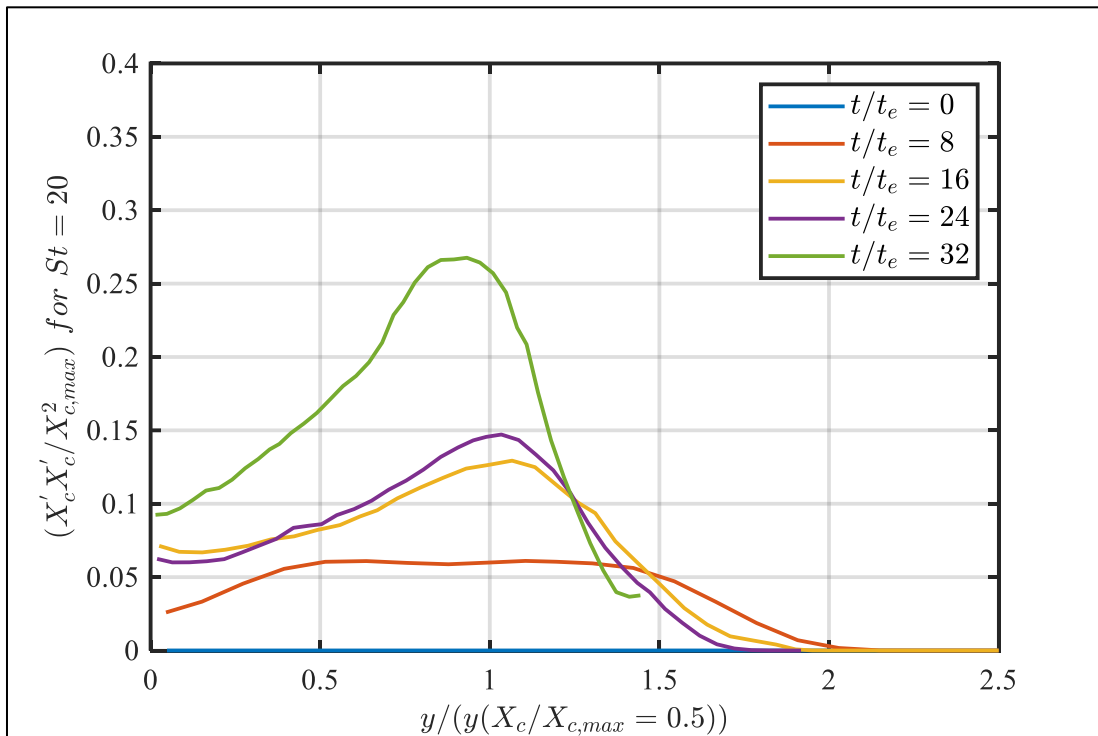
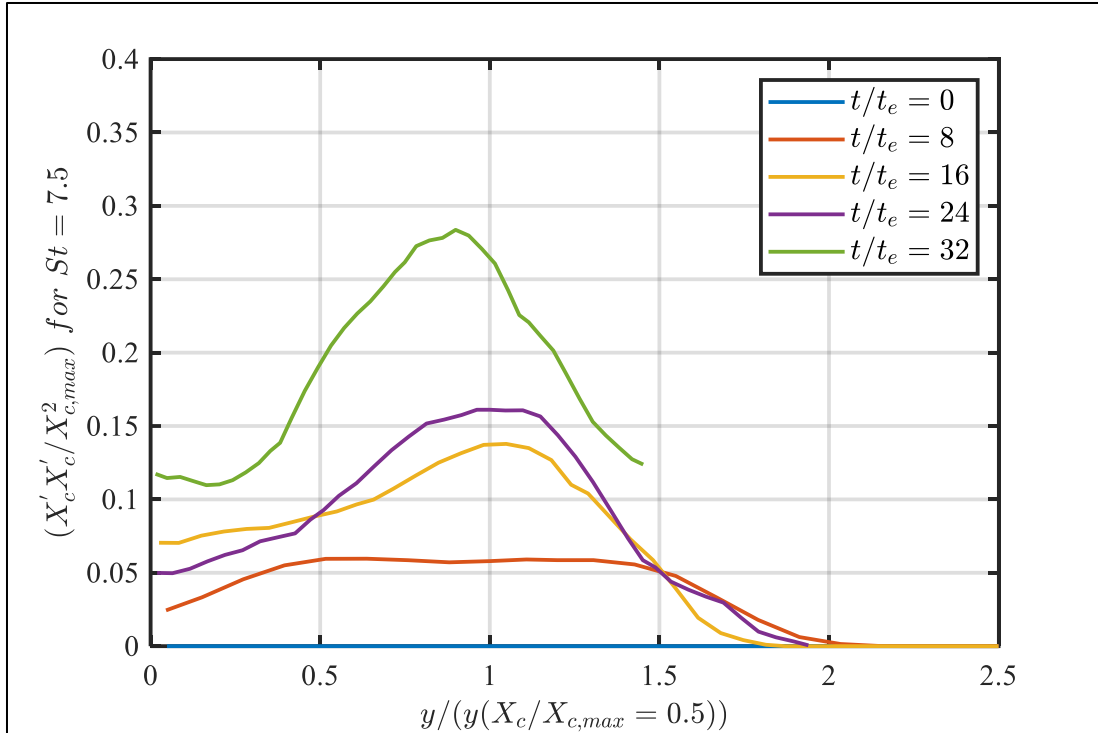


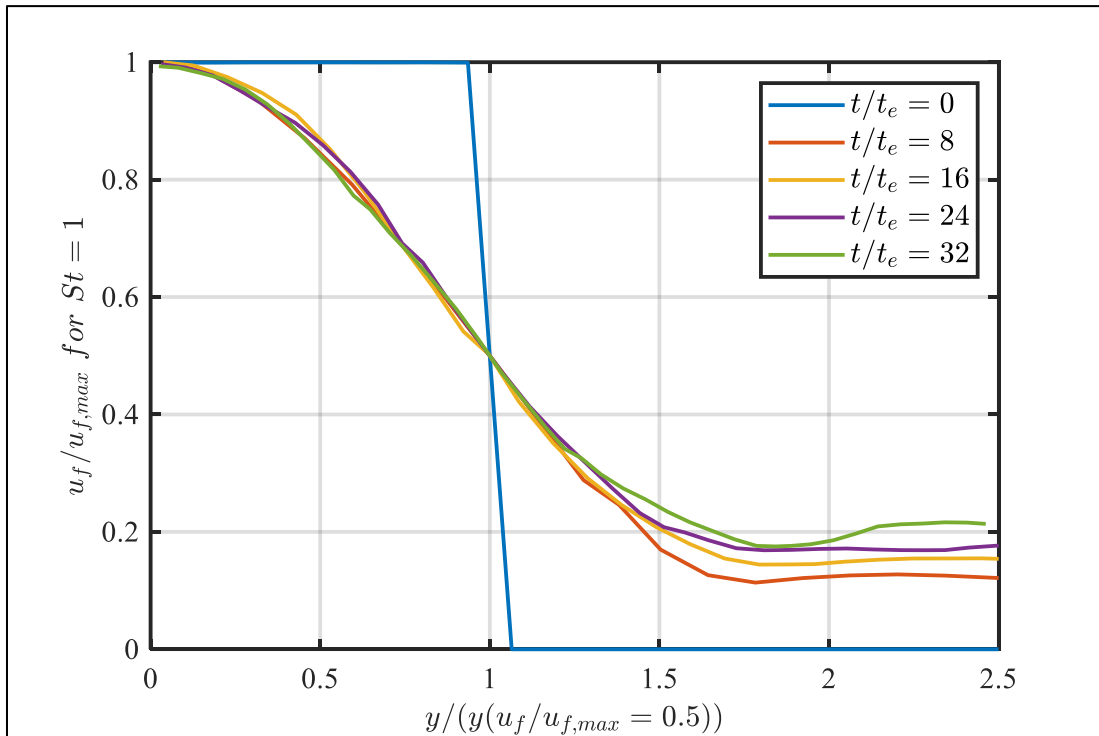
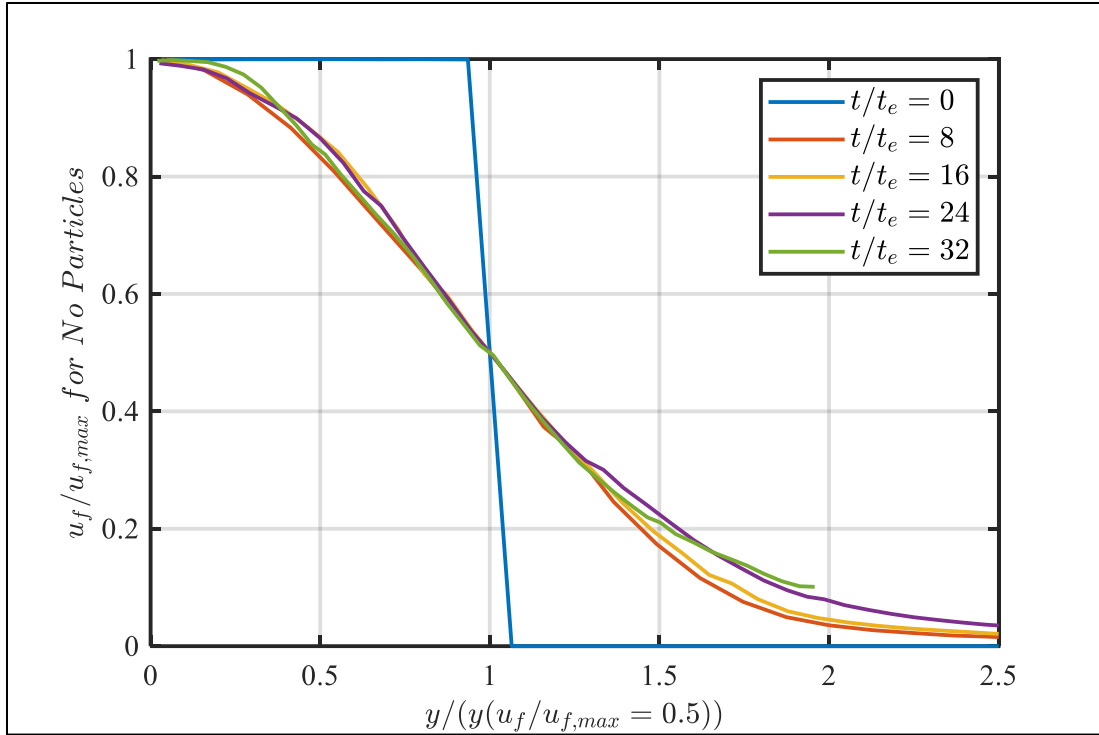
(Fig 4.4.2 – Variance of Mixture fraction over time for

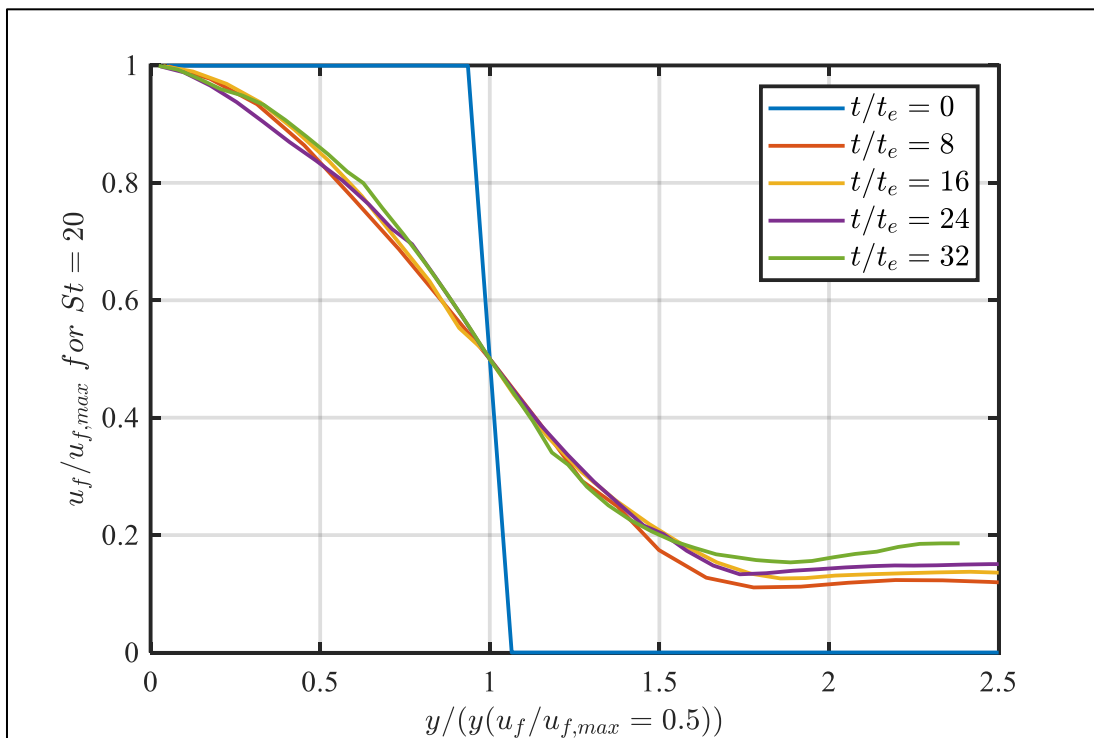
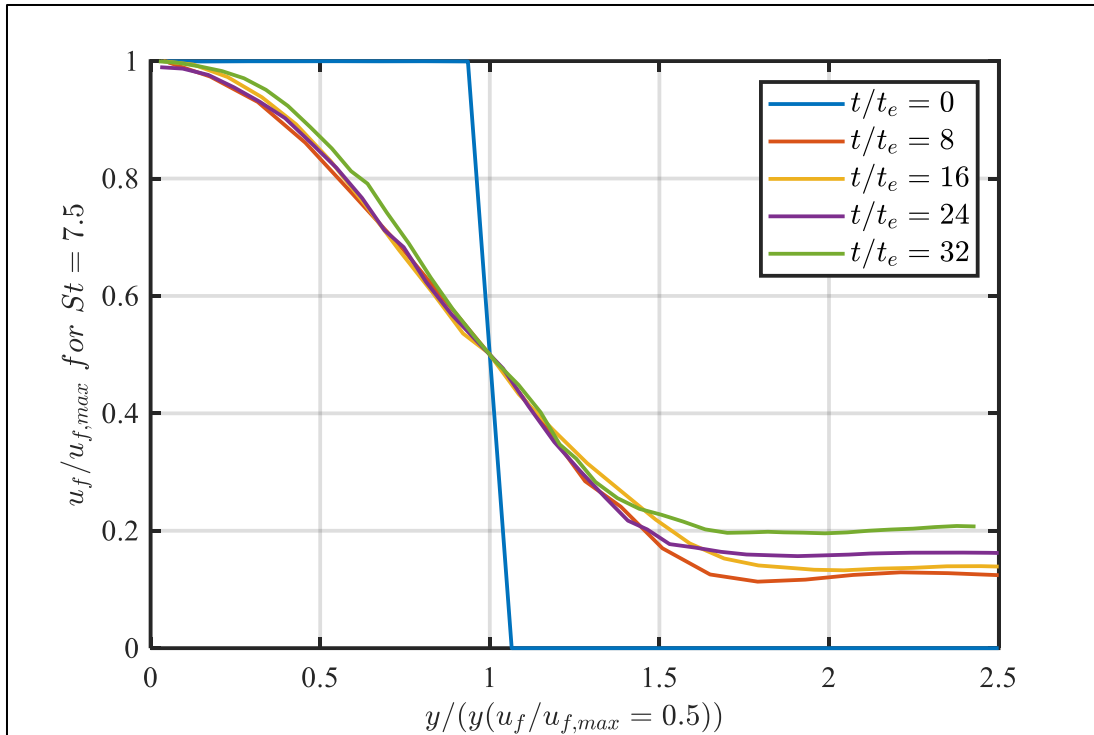
(a) No Particles, (b) $St = 1$, (c) $St = 7.5$ and (d) $St = 20$)

From Fig 4.4.2, the maximum variance in the scalar mixture fraction is getting shifted from edge of the jet width to away from it as t progresses. The peak value of the variance decreases and the variance curve from the domain center to the peak is shifted downwards with increase in St . Also, the slope of the variance curve from peak to the domain boundaries is depicted by the St and decreases with increase in St .

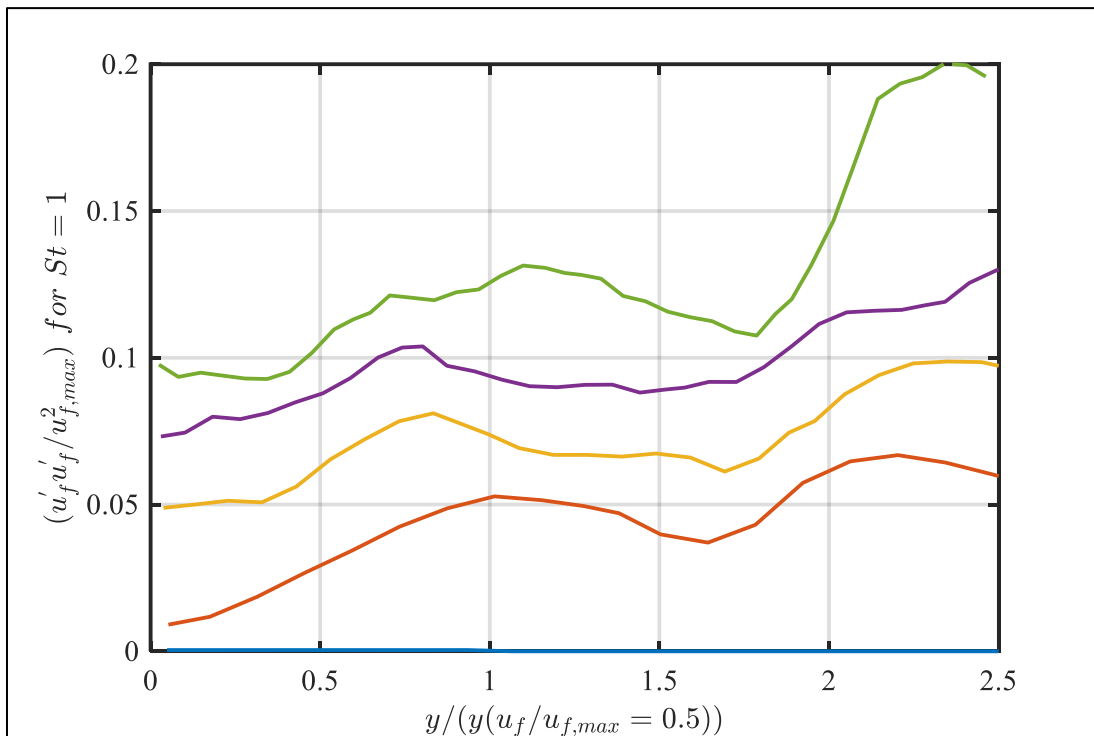
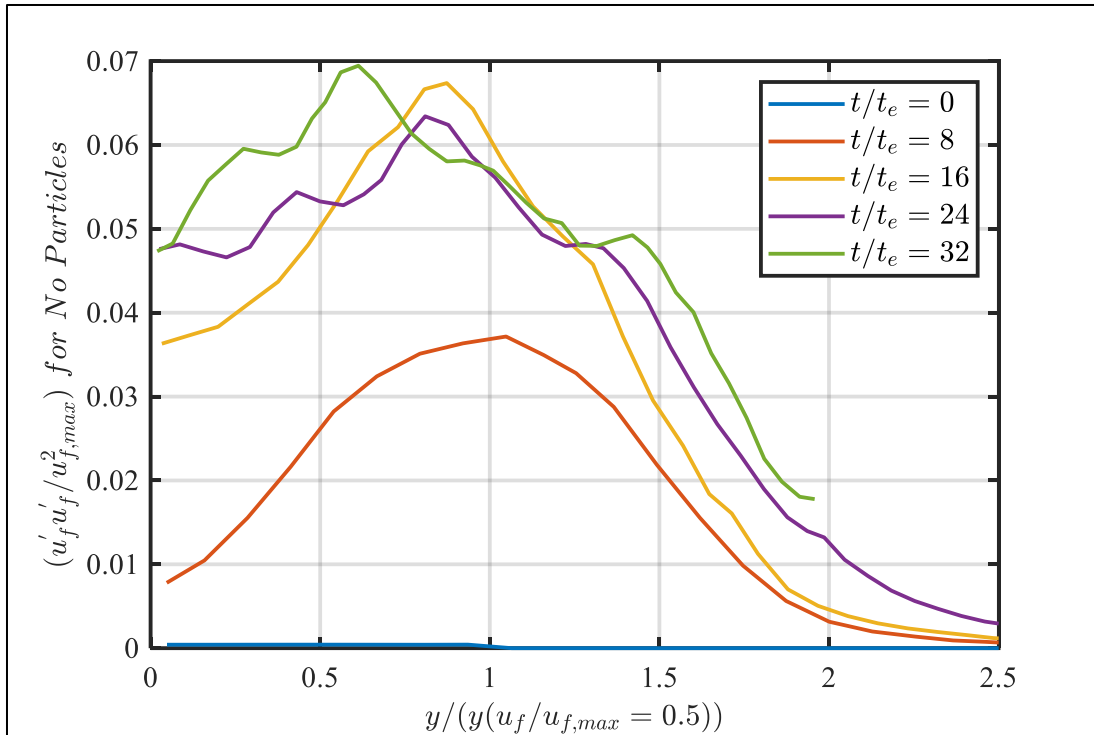
After the mixture fraction, the streamwise jet velocities (u_f) for different St are analyzed and plotted in Fig 4.4.3. For various St , there is no significant change in the cross-stream velocity profile, but there is an observable difference in comparison of the particle-laden case with particle-free case. It is observed that the fluid in the quiescent domain is also accelerated to a certain velocity ($\sim 15\%$ of the jet velocity). This reason for this difference is attributed to the pressure solving term in the particle-transport equation. The pressure term in the particle transport equation is significant during the earlier time-steps, that causes the particles in the non-jet domain to move. This in turn causes the fluid in the non-jet domain to move with this smaller amount of velocity until the jet dissipates itself into the region. This trend is also observed in streamwise variances and TKE.

The variances of streamwise, crosswise and spanwise velocities are plotted in Fig 4.4.4, 4.4.5, and 4.4.6 respectively. The streamwise velocity variance doesn't converge at the edge due to the above effect and generates a local peak at around jet velocity half-width and local minima at nearly 1.75 times of jet velocity half-width. This is not the case for particle free case which has only one maximum that is at jet velocity half-width. Also, from Fig 4.4.4., the turbulence along the streamwise velocity decreases with increase in the St .





(Fig 4.4.3 – Spanwise velocities of the jet fluid for (a) No Particles, (b) $St = 1$, (c) $St = 7.5$ and (d) $St = 20$)



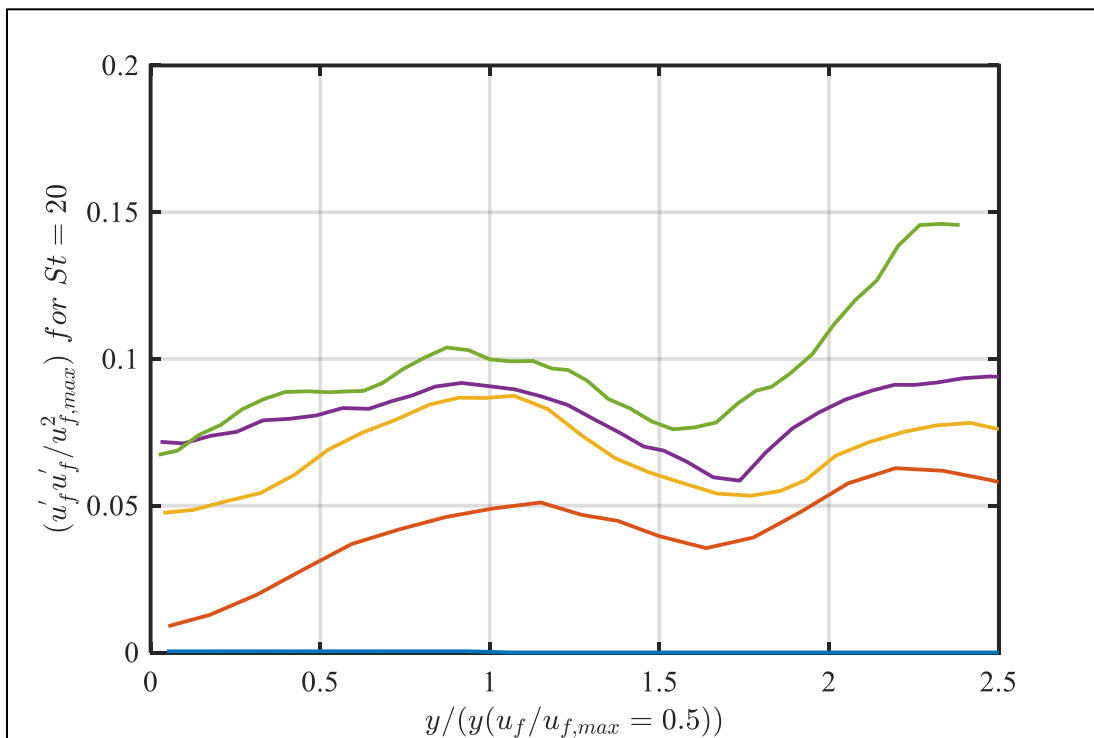
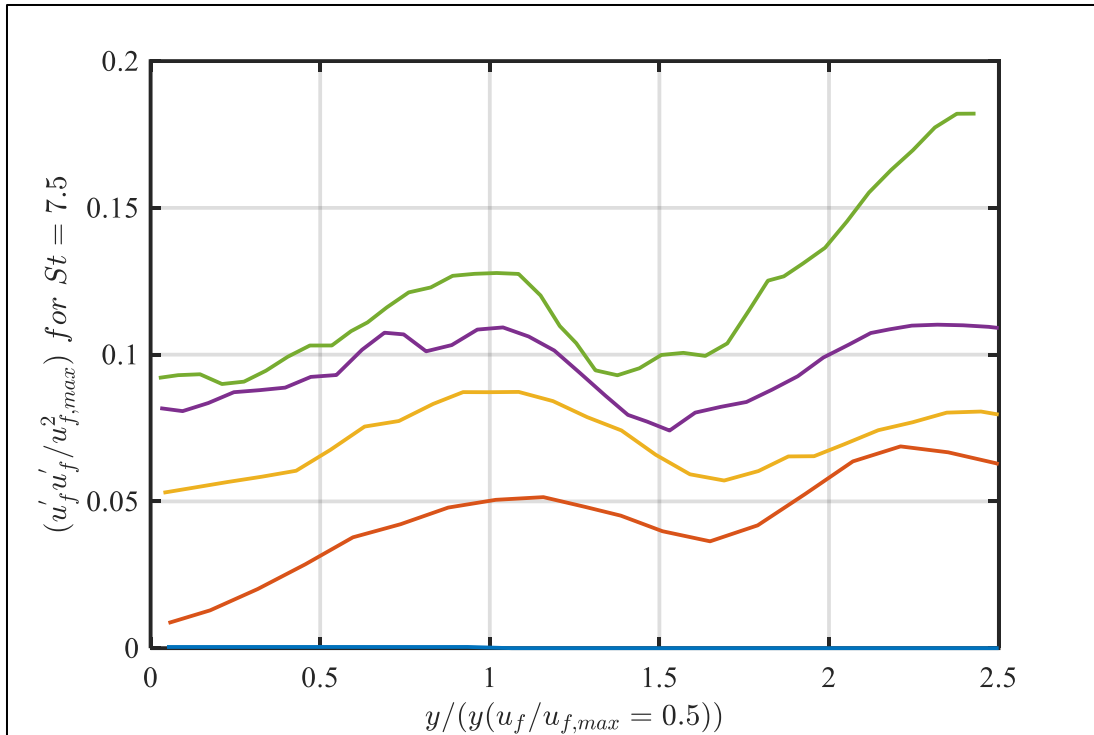
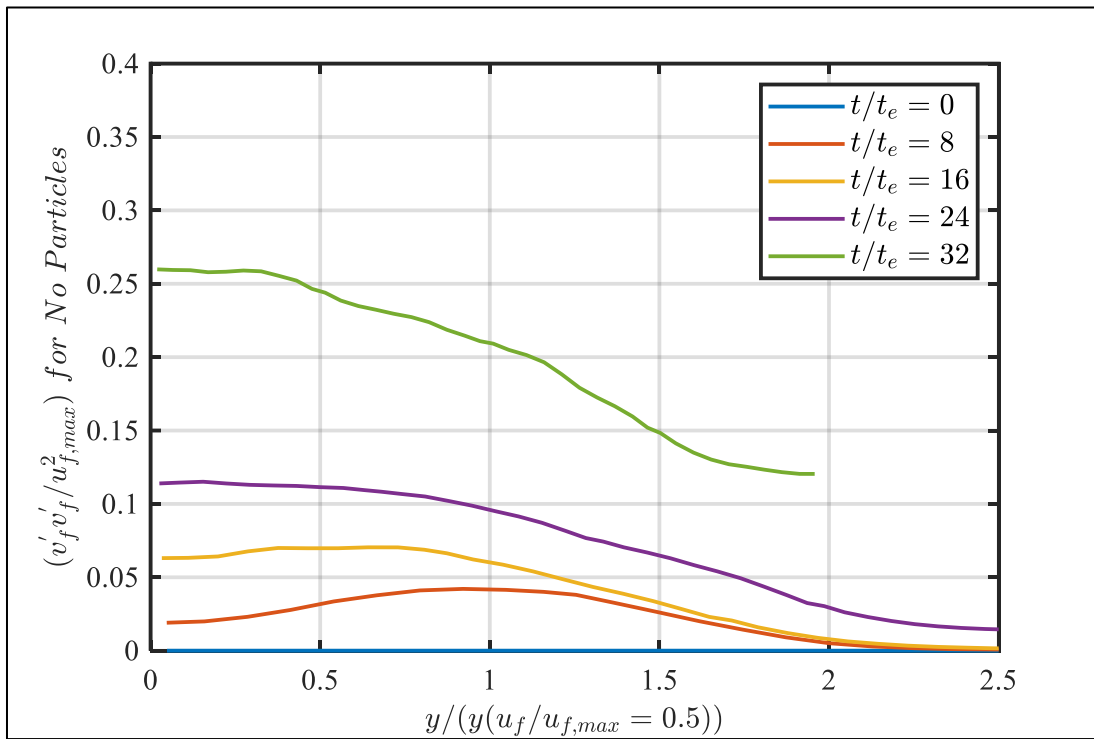


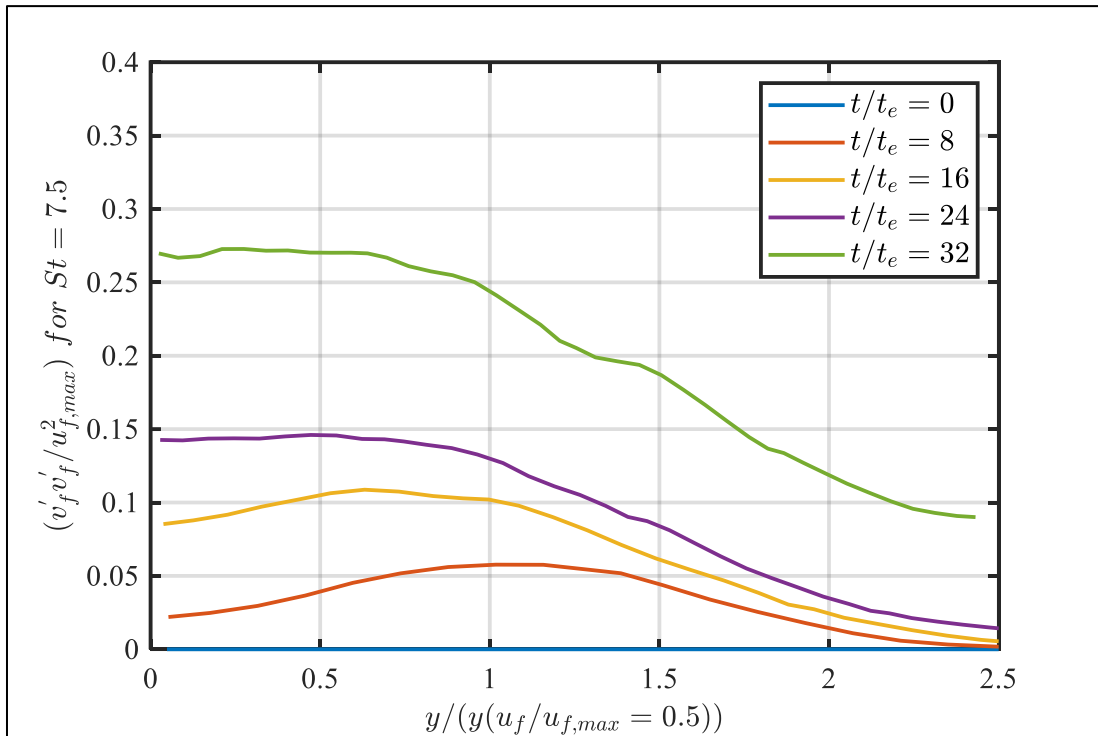
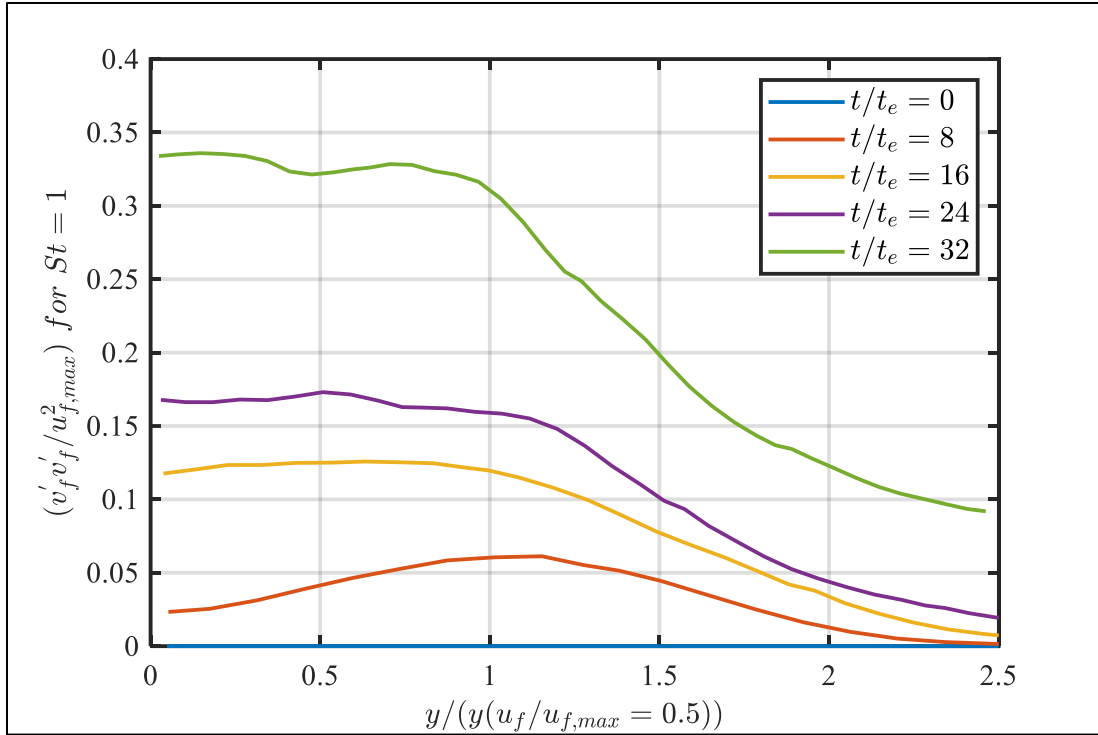
(Fig 4.4.4 – Variance of the jet velocity in Streamwise direction for

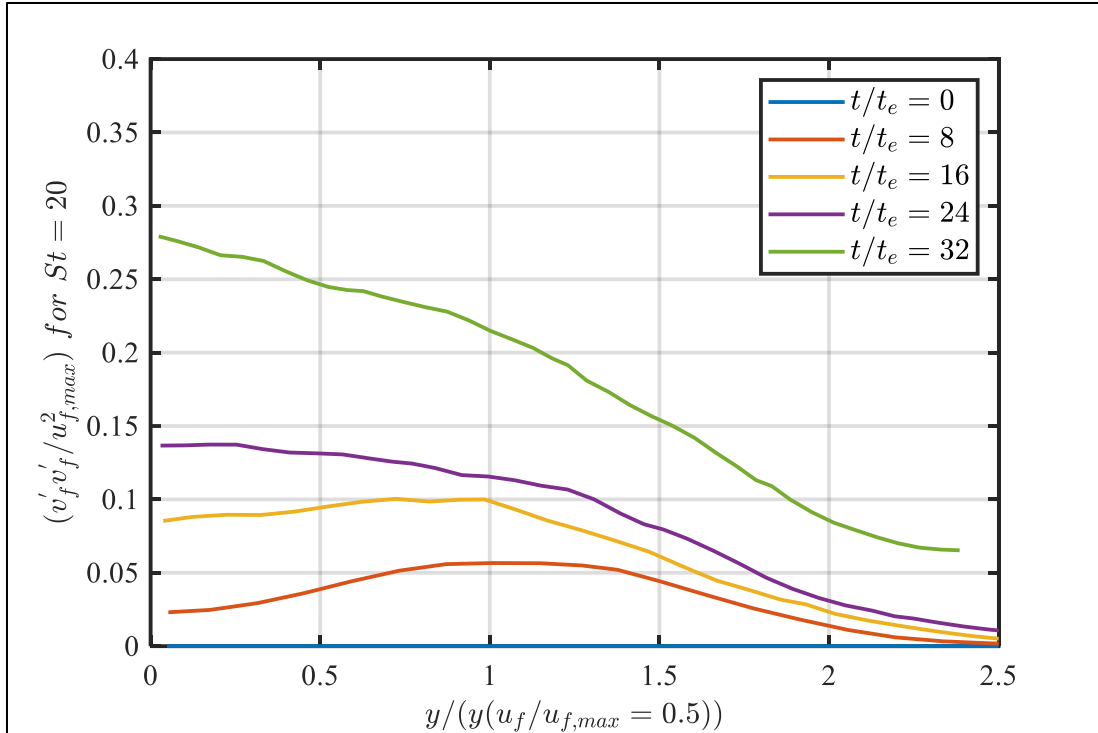
(a) No Particles, (b) $St = 1$, (c) $St = 7.5$ and (d) $St = 20$)

From Fig 4.4.5 and 4.4.6, the cross-stream and span-wise velocity variances for the particle-laden case shows the same convergence of the particle-free case. In-case of the cross-stream wise velocity variance, the maximum occurs at the center-plane irrespective of the St . Where as in-case of span-wise velocity variance, the maximum occurs at the jet velocity half-width which is at the same spot of that of the stream-wise velocity variance plots in Fig 4.4.4 without considering the pressure affects.

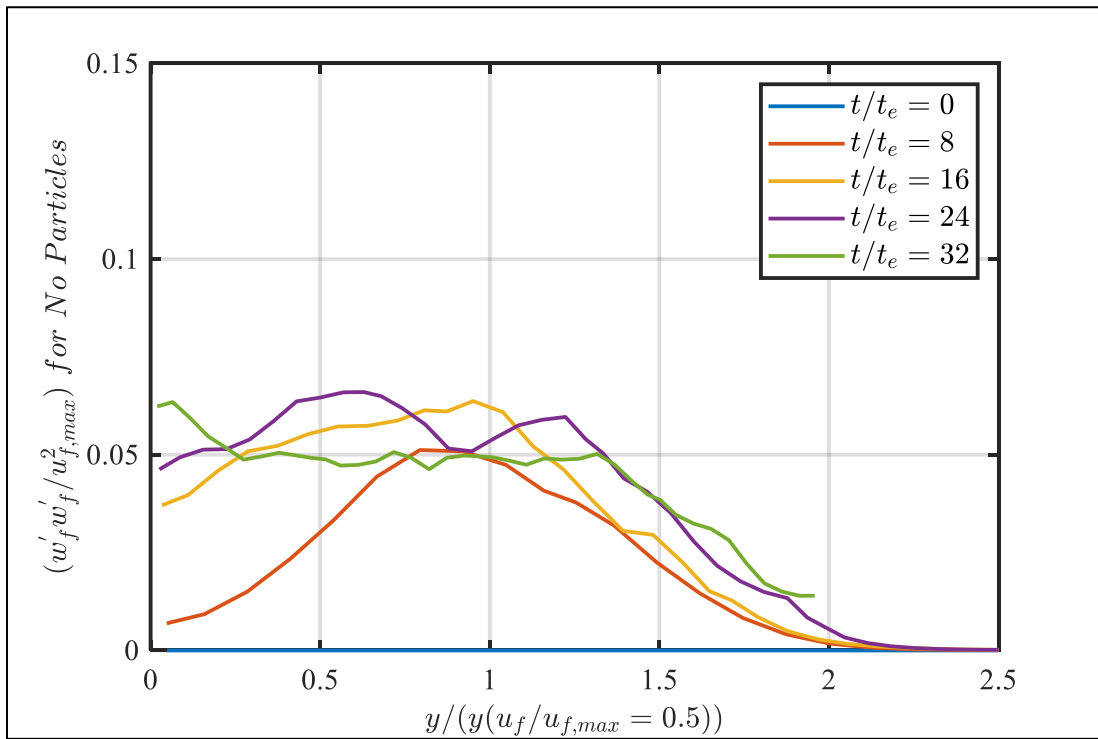
For the cross-stream turbulence fluctuations trends, from Fig 4.4.5, the turbulence fluctuations variances are comparatively more with $St = 1$ rather than at lower and higher St . For the spanwise turbulence variance, from Fig 4.4.6, the variance for particle free case is very low when compared to that of the particle-laden case but there is no significant difference that can be observed from different St .

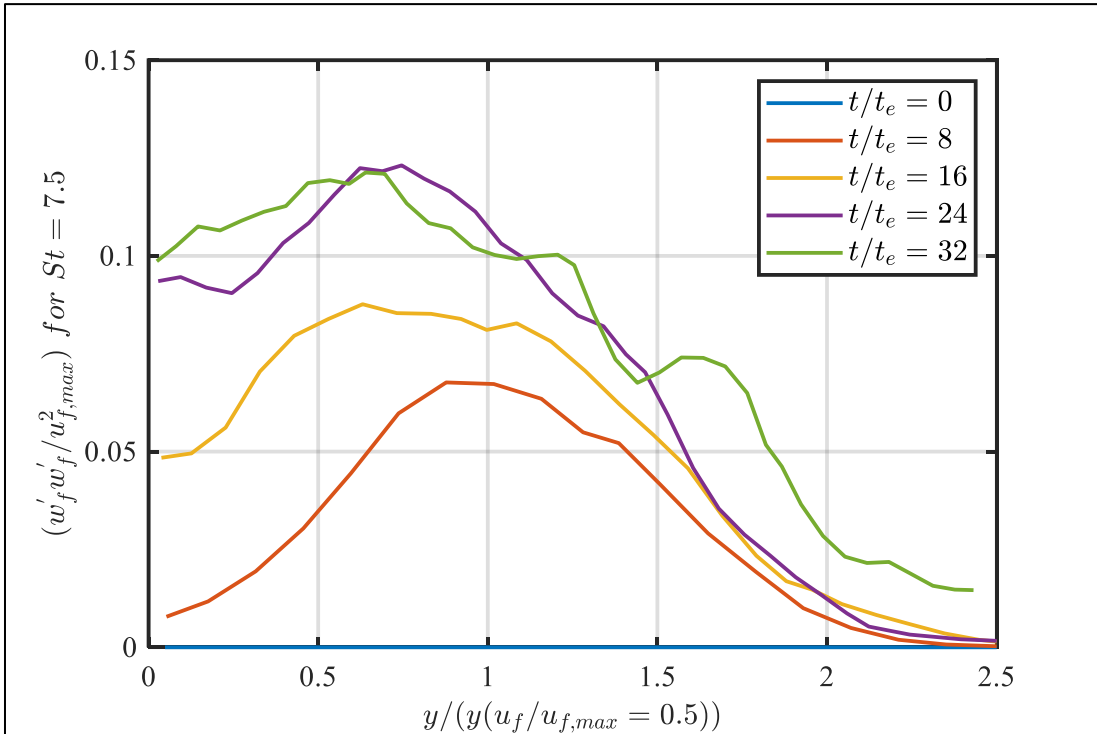
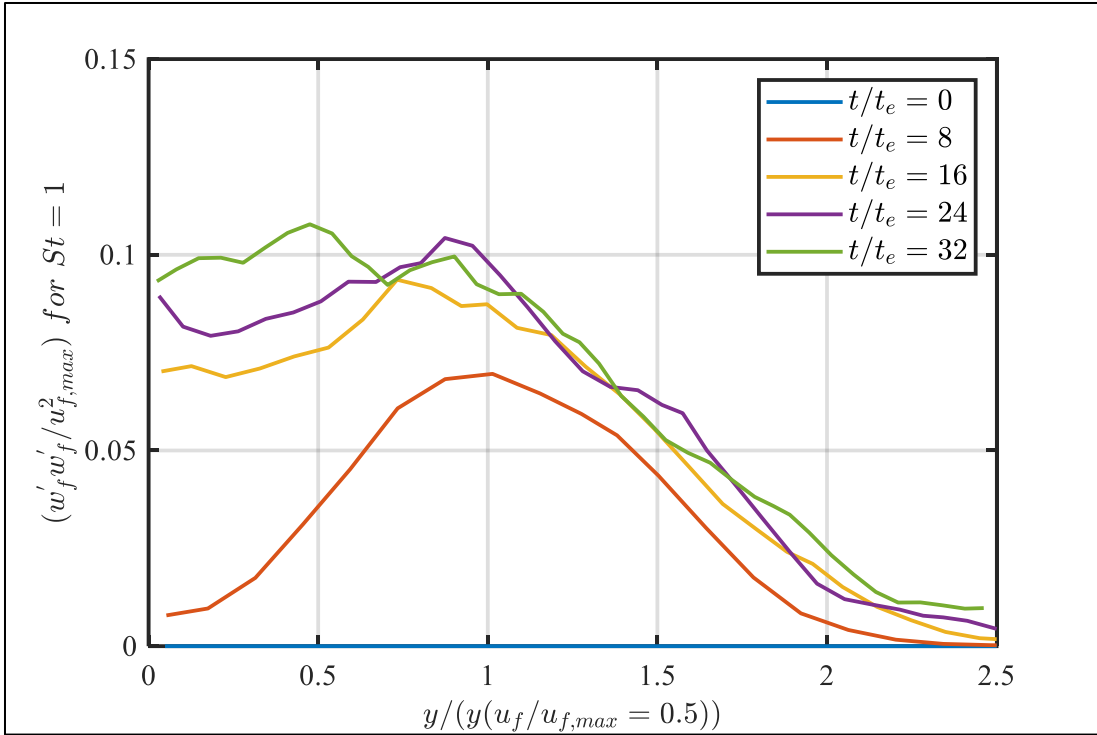


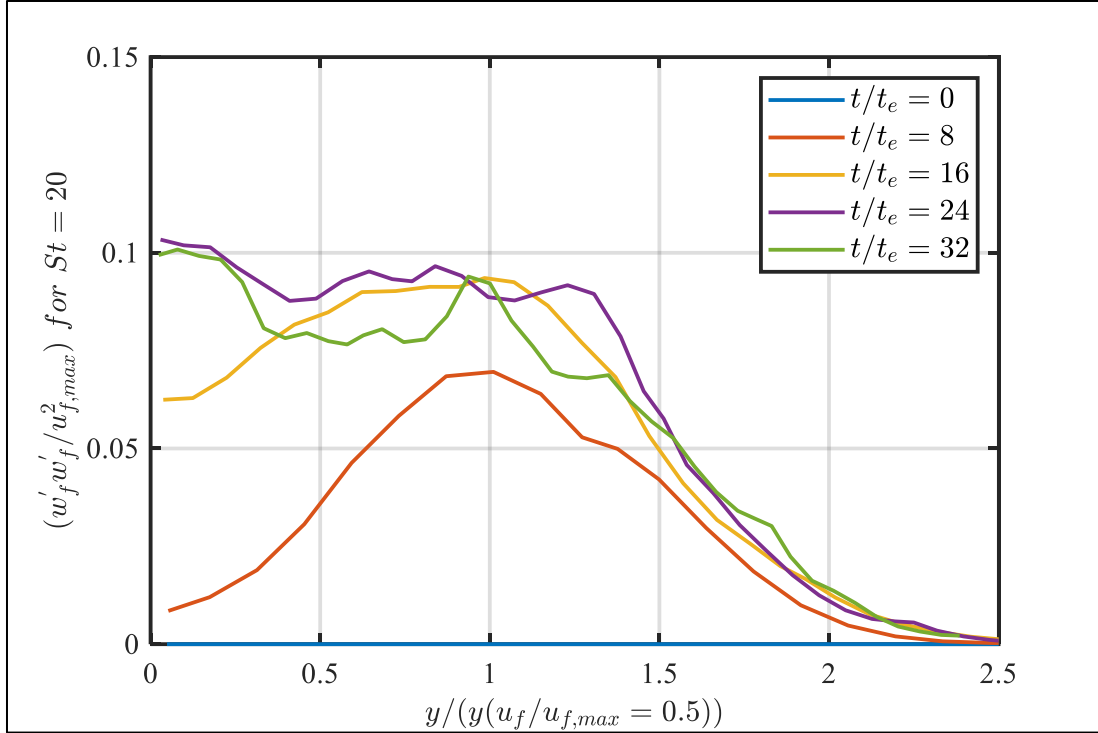




(Fig 4.4.5 – Variance of the jet velocity in Cross-stream direction for (a) No Particles, (b) $St = 1$, (c) $St = 7.5$ and (d) $St = 20$)

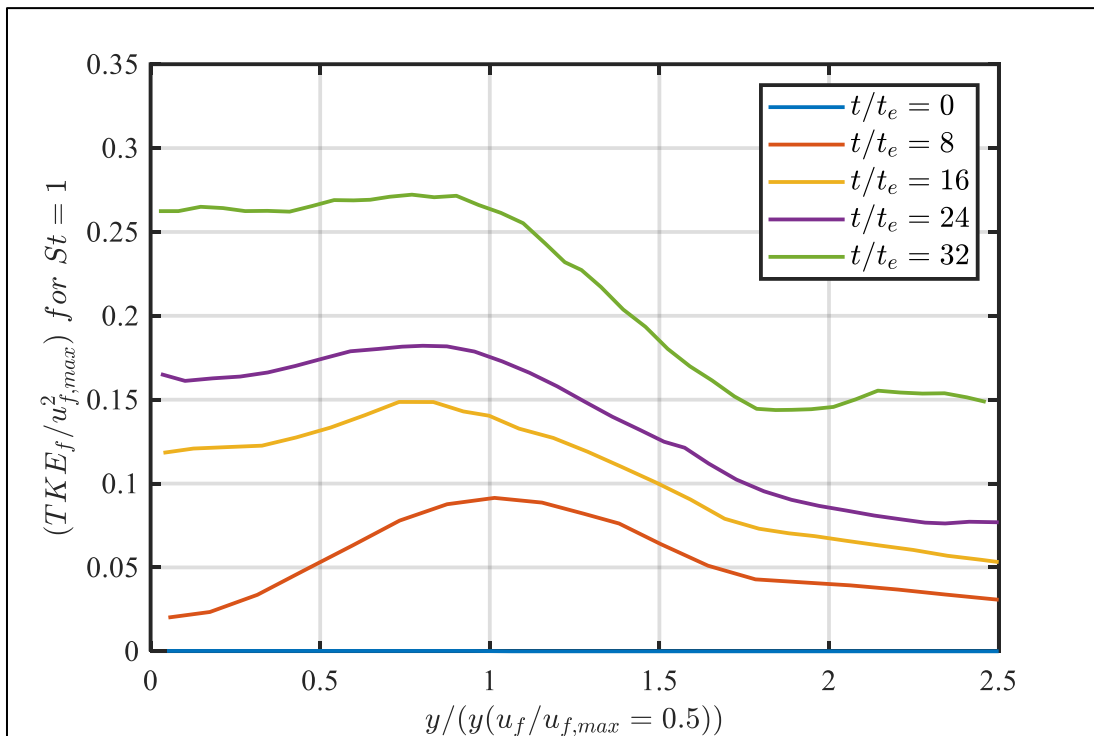
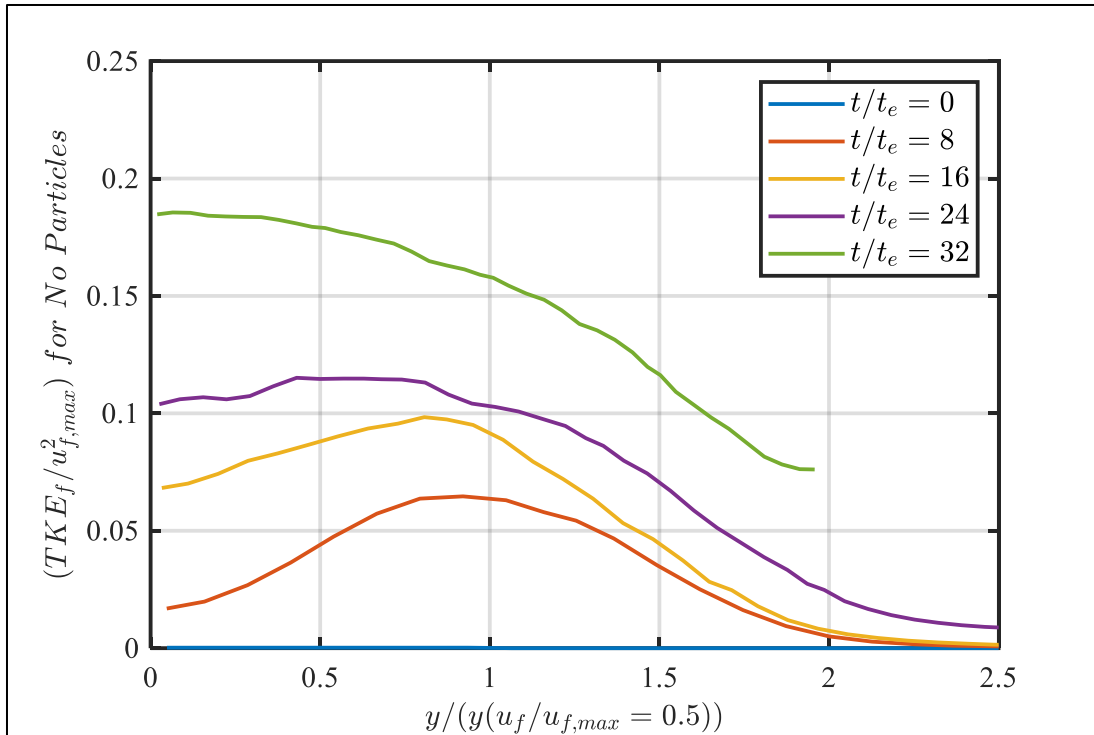


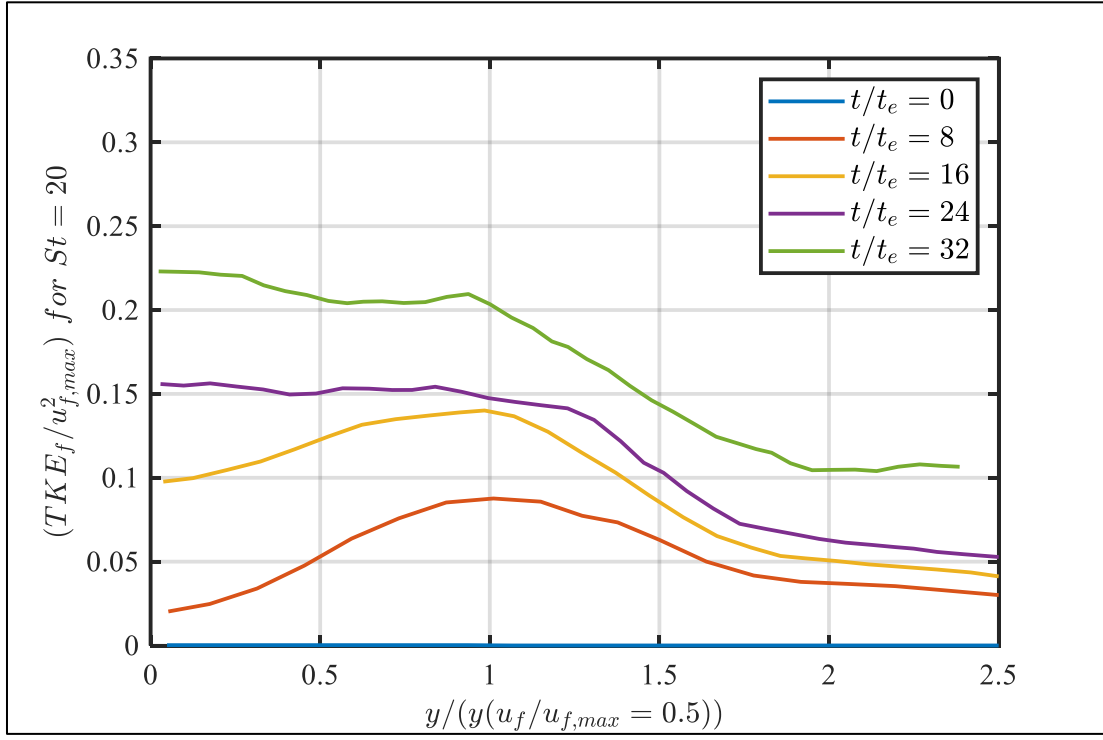
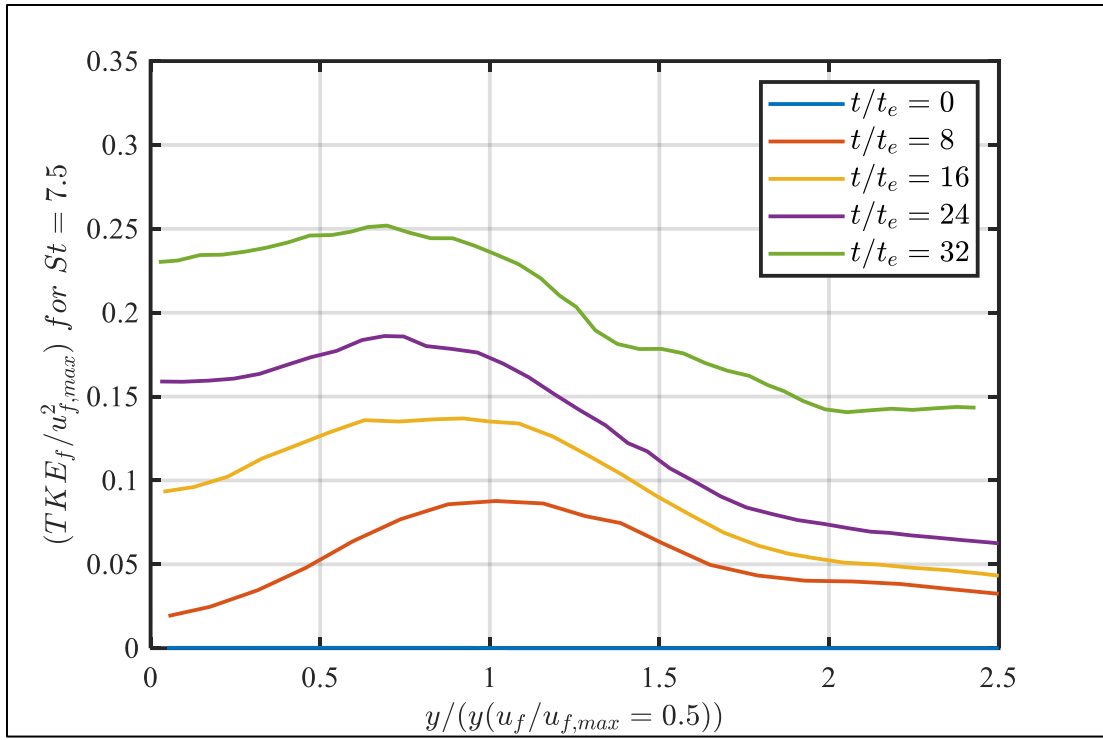




(Fig 4.4.6 – Variance of the jet velocity in Span-wise direction for (a) No Particles, (b) $St = 1$, (c) $St = 7.5$ and (d) $St = 20$)

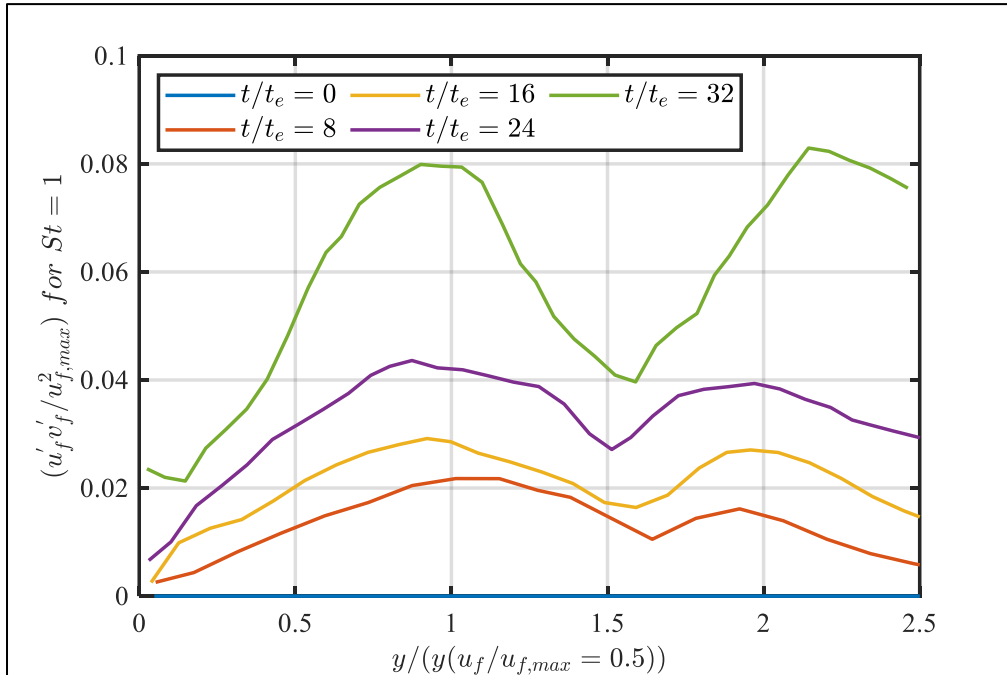
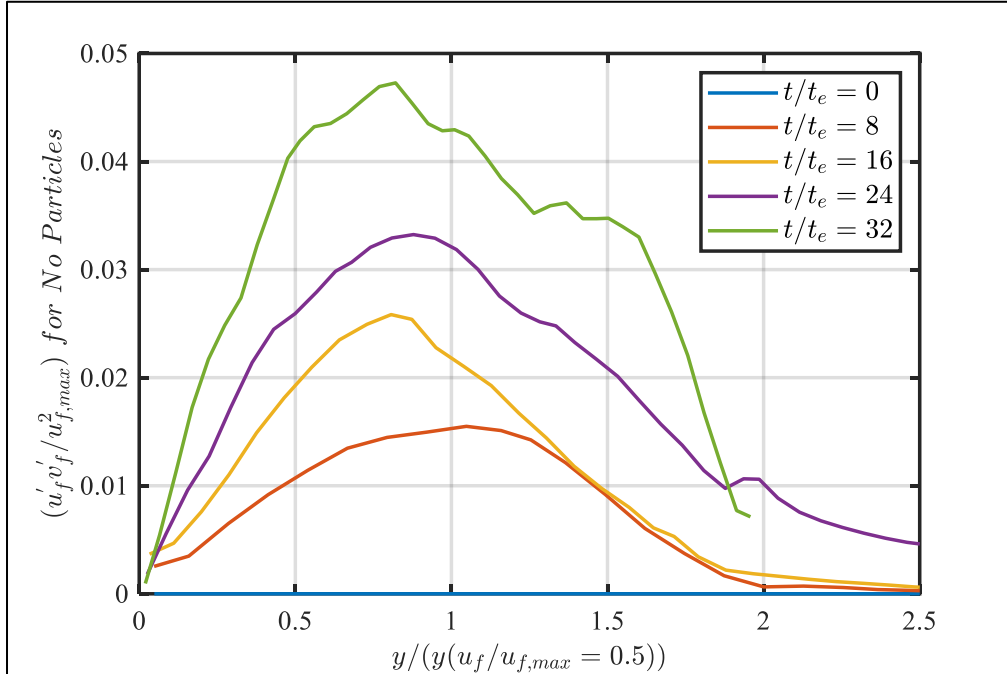
The above variances are appropriately added to estimate the TKE_f for different St and are plotted in Fig 4.4.7. The TKE_f values at the near boundary domain region for particle-laden case are not converging to 0 as that of the particle-free case. This is because of the pressure term as discussed during the jet velocity profile at Fig 4.4.3. Apart from this non-convergence, there is only a maxima peak observed in all the cases. This peak exists closer to the jet velocity half-width. The trend of TKE_f between different St for streamwise-normal case matches with that of the streamwise-parallel one. This could be inferred that the TKE_f profile and value at certain location increases till $St = 1$, compared to the particle-free and higher St , indicating that an optimal St exists for which the scalar variation is maximum at any instant of time.





(Fig 4.4.7 – Turbulent Kinetic Energy of the jet (TKE_f) for (a) No Particles, (b) $St = 1$, (c) $St = 7.5$ and (d) $St = 20$)

Unlike the streamwise-parallel plane case where the covariance terms are zero, in the streamwise-normal plane one of the co-variance terms ($u'_f v'_f$) is non-zero. The plot for the Reynolds shear stress, R_{uv} is plotted in Fig 4.4.8.



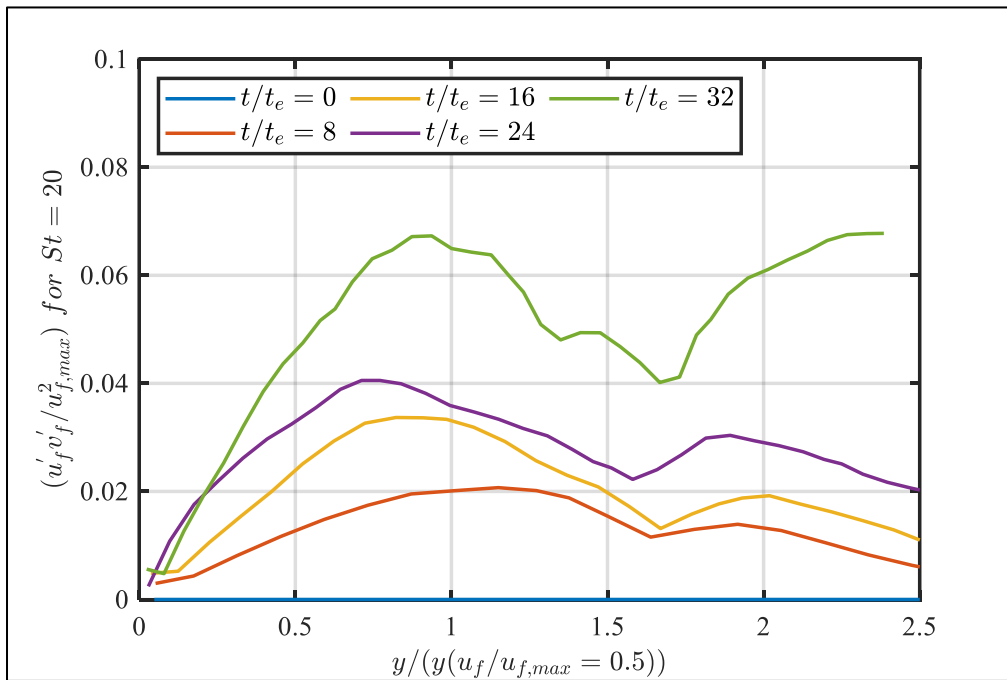
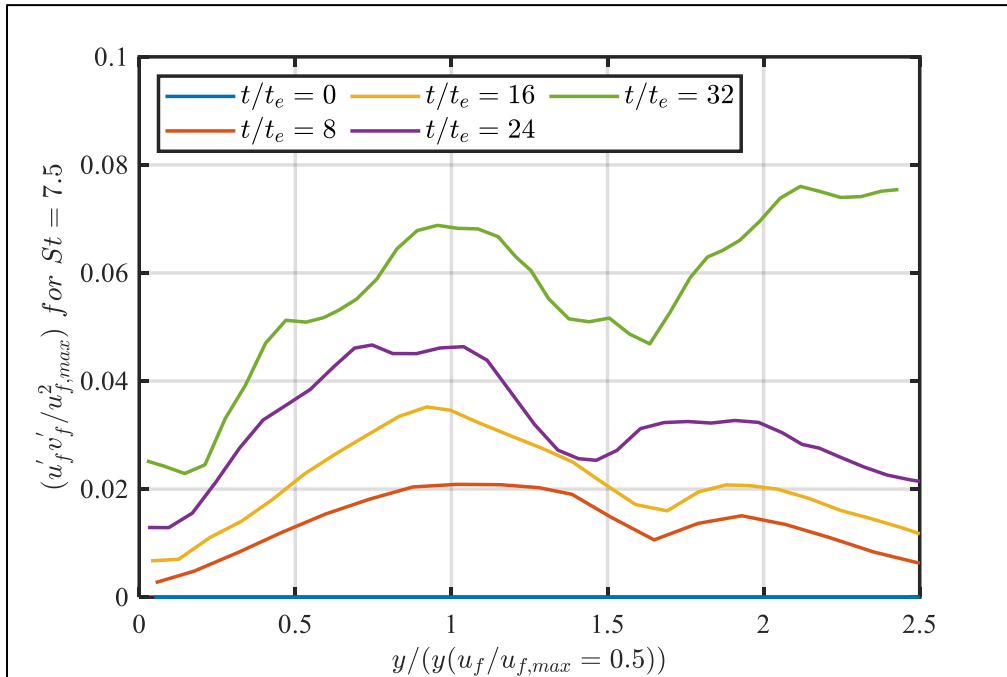


(Fig 4.4.8 – Co-variance $(u'_f v'_f)$ of the fluid for
 (a) No Particles, (b) $St = 1$, (c) $St = 7.5$ and (d) $St = 20$)

From Fig 4.4.8, the peak of the co-variance also occurs near to the edge of the jet half-width which is similar in-comparison with the TKE_f . The co-variance plot converges to 0 at smaller time but it diverges for the larger time for particle-laden case hinting at the pressure term issue. When the Fig 4.4.8 plots are analyzed for a certain time and certain location, the same trend of the TKE_f in Fig 4.4.7 can be noticed. The noticed trend is that the co-variance value for $St = 1$ is more at a fixed time and location in-comparison with lower and higher St . This suggests that $St = 1$ is an optimal solution where the turbulence occurs significantly higher resulting in better mixing when compared to other St .

Hence when streamwise parallel (or) streamwise normal plane is considered, the variance of mixture fraction, TKE_f and Reynolds stresses are comparatively higher around $St = 1$ when compared to other St that are away from $St = 1$. This implies that for $St = 1$ effective exchange of turbulence between the particles and fluid occurs causing more scalar variance and ultimately effective mixing.

4.5 – Qualitative Analysis of Particles Clustering

After the qualitative analysis of the fluid flow and statistical analysis along various planes, the qualitative analysis of the particles is studied to understand the clustering effect of the particles in the domain. A single layered particle plots are generated for both $St = 1$ and $St = 20$ and are overlaid on (1) Velocity and (2) Mixture fraction plots at $\sim 14t_e$ respectively, as shown from Fig 4.5.1 to Fig 4.5.4. From Fig 4.5.1 and 4.5.2, the particles can be observed to be passively moving with $St = 1$ whereas particles are not moving in phase with the fluid for $St = 20$.

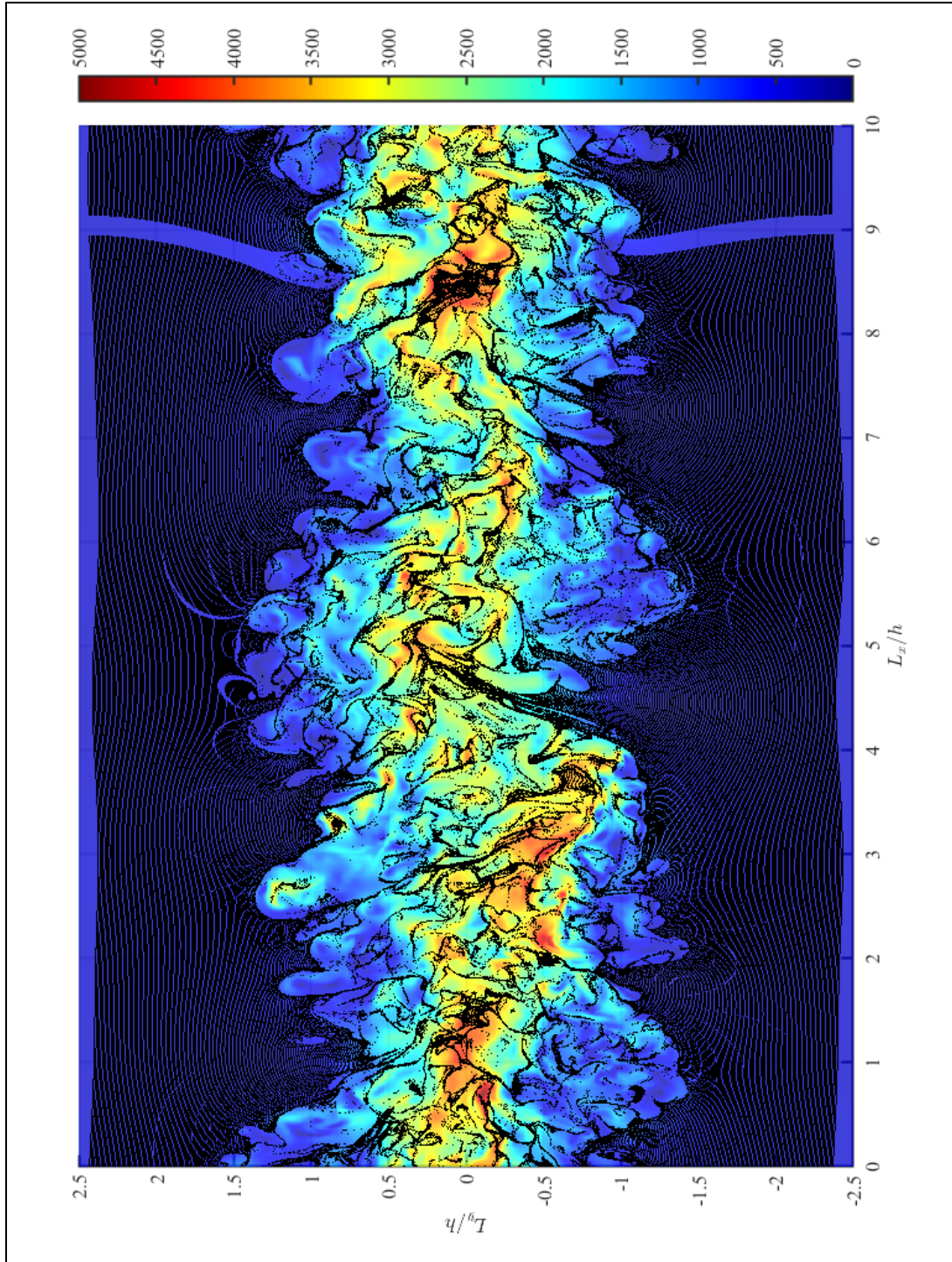


(Fig 4.5.1 – Single layered particle plot overlaid on fluid velocity for $St = 1$)

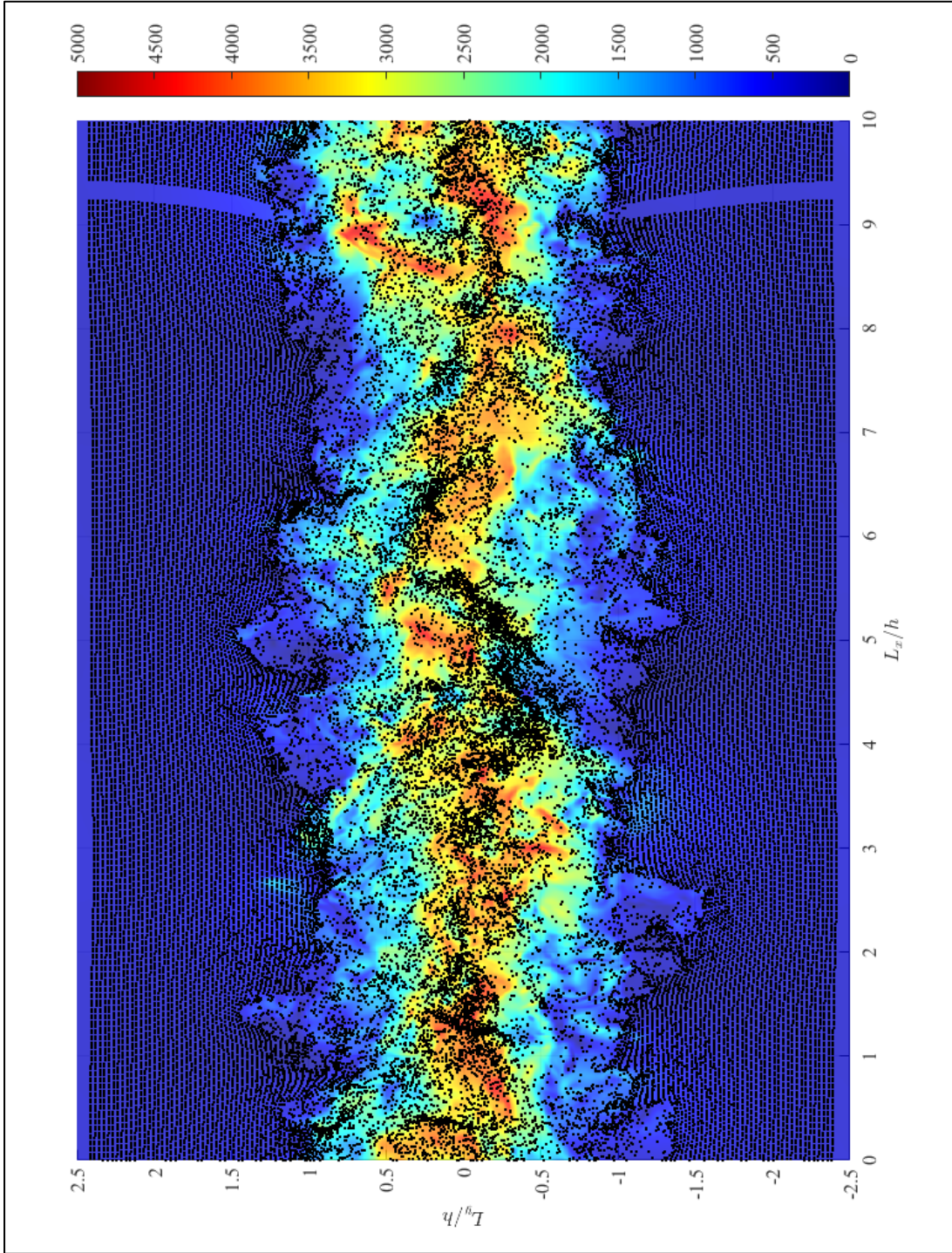


(Fig 4.5.2 – Single layered particle plot overlaid on fluid velocity for $St = 20$)

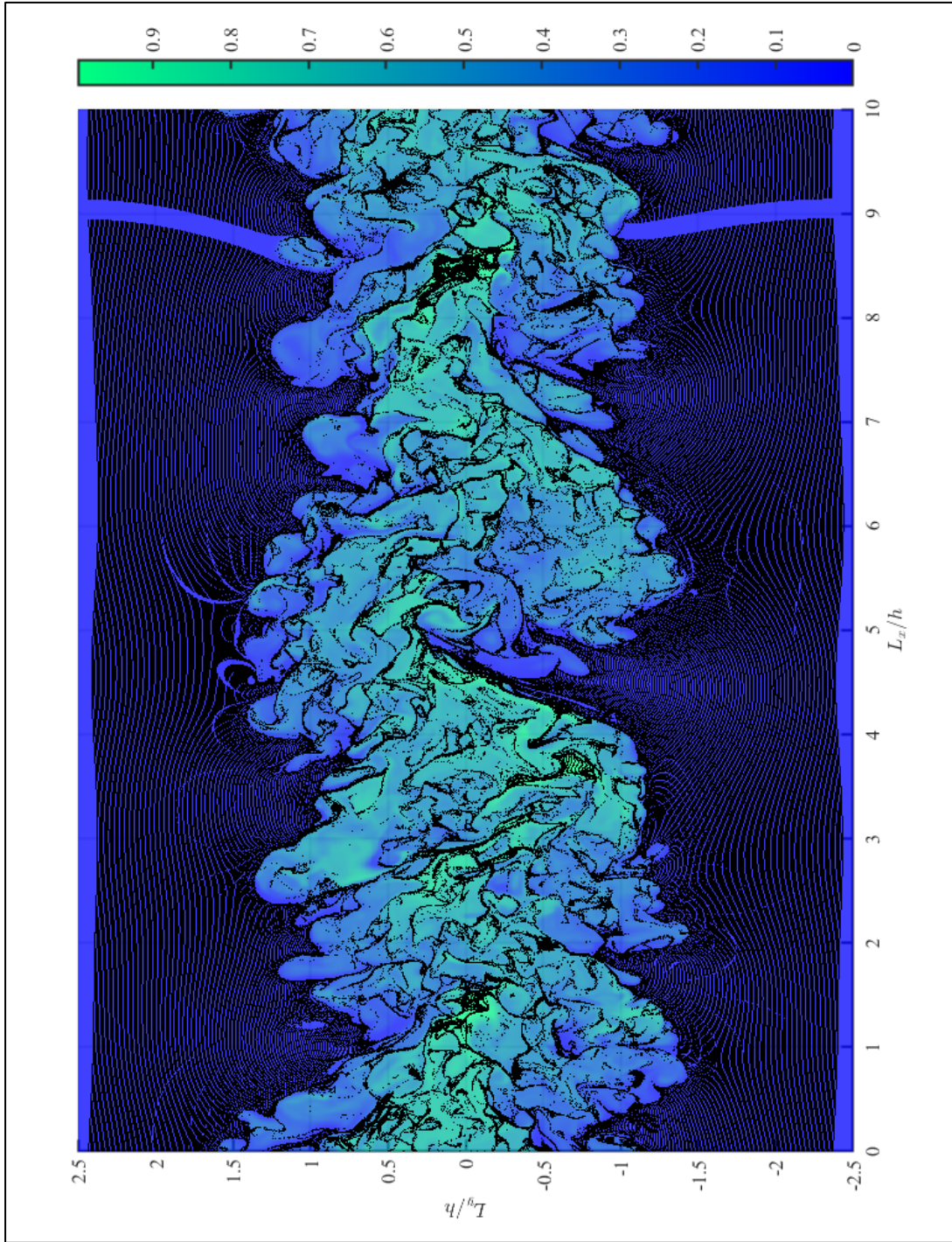


(Fig 4.5.3 – Single layered particle plot overlaid on Mixture fraction for $St = 1$)

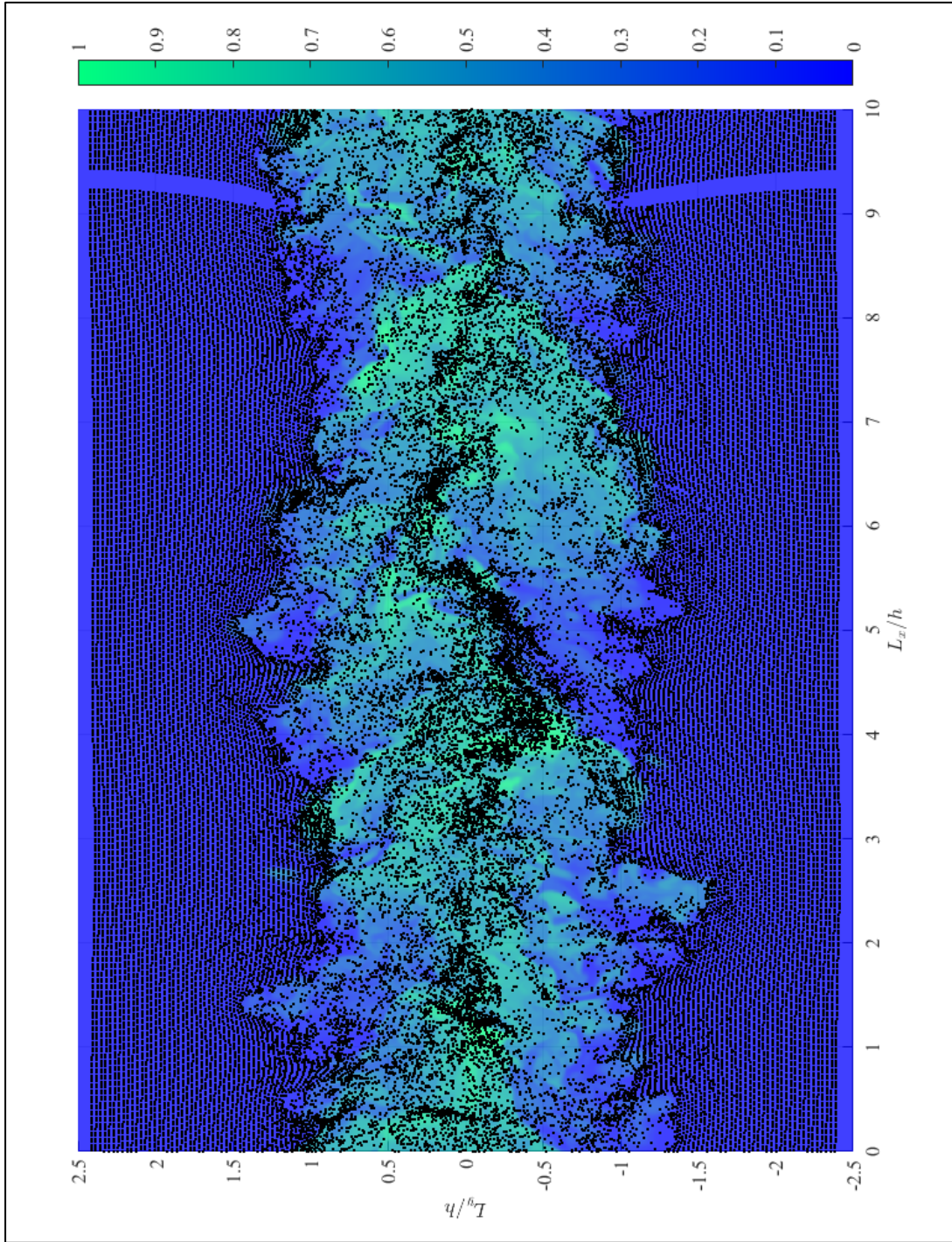


(Fig 4.5.4 – Single layered particle plot overlaid on Mixture fraction for $St = 20$)

From Fig 4.5.3 and 4.5.4, It can be observed that the jet pushes some of the particles to the jet and non-jet interface boundary. Apart from the interface boundaries, the particles clustering can be found near the centerline of the jet, where there is almost uniform and higher value of velocity or concentration. This implies that the particles clustering can also be found near to the centerline spots where the jet velocity or concentration is a little bit high and almost constant which also corresponds to higher velocity and lower velocity gradient between the surrounding flow.

4.6 – Statistical Analysis of Spread Rates

One of the best ways in determining the spread rate is through estimation of jet half-widths. In this work, 2 jet half-widths based on – (1) velocity, and (2) scalar concentration, are estimated and the graphs are plotted in Fig 4.6.1 and Fig 4.6.2 respectively.

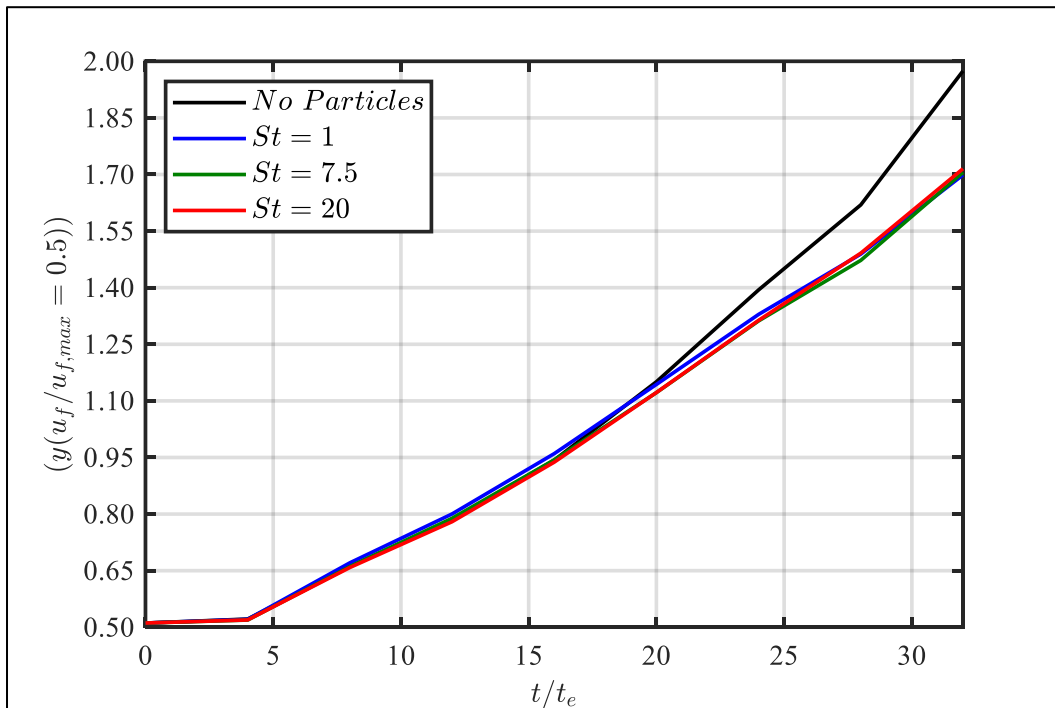


(Fig 4.6.1 – Time series of jet velocity half-width for different St)

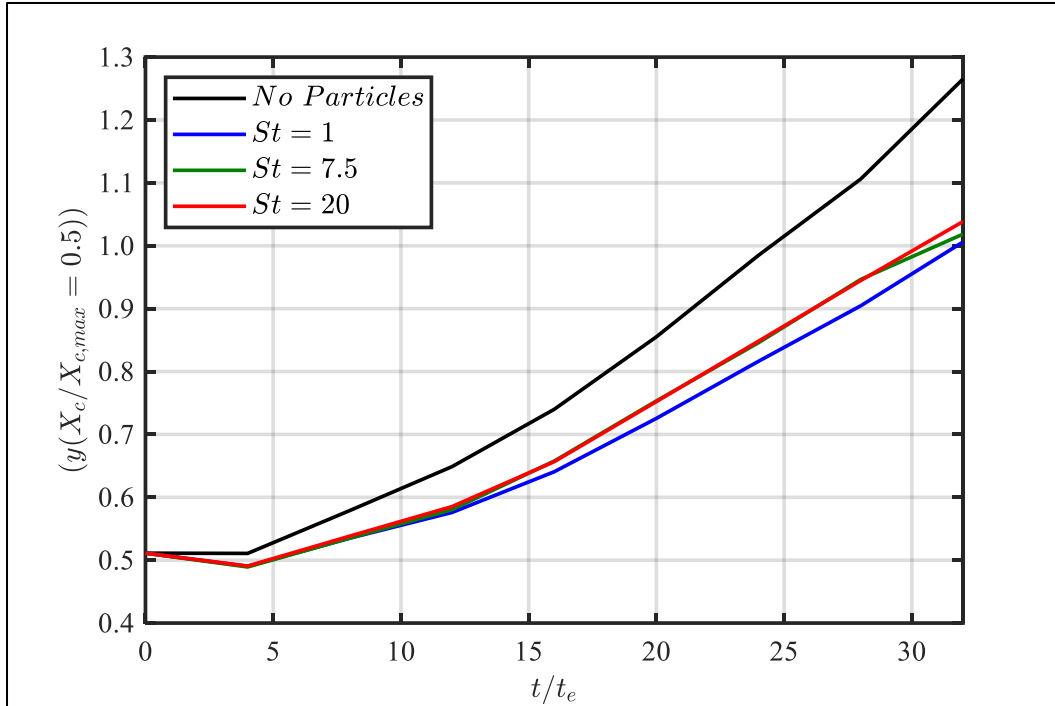


(Fig 4.6.2 – Time series of jet concentration half-width for different St)

From Fig 4.6.1, There isn't any significant difference between the velocity jet half-widths of different St . This implies that the mean velocity profile of the jet is almost constant and hence no difference in velocity spread can be observed for different St . Although the velocity half-width shows no significant difference for different St , it is different in case of concentration half-width, that can be observed from Fig 4.6.2. The jet concentration half-widths are not significantly different, but comparatively $St = 1$ shows a little less jet half-width when compared to other St .

CONCLUSIONS & FUTURE WORK

In this thesis work, the effect of the particles on the temporal jets is being studied and developed with the help of the Navier-Stokes equation and the advection-diffusion equation with appropriate grid sizes such that the smallest length scales of the turbulence are captured when the DNS is performed on the computation domain. The smallest possible eddies are seen when the grid size is less than the Kolmogorov length scale. To maintain this criterion to capture the simulations were carried out with ~ 0.5 billion grid points and took nearly 5 days for each simulation to run till each case of the Stokes number completes nearly $60t_e$. Although the simulation is carried out till $60t_e$, after nearly $35t_e$ the effect of domain constraints in the cross-sectional planes come into the picture, disturbing the free shear turbulence that is occurring in the domain. Hence the simulations were analyzed till $35t_e$ to better understand the undisturbed turbulence phenomenon from the boundaries for the temporal jet in the particle-laden domain.

The qualitative results of the cross-stream flow depict the motion of the scalar concentration of the jet in the domain. It also supports in establishing the results of lesser jet spreading in-case of higher St in-comparison with the lower ones. Also, most of the particles move (or) have the velocity in-case of smaller St , whereas only some of the particles show movement in higher St case.

Also from the particle clustering results, it can be inferred that the particle clusters are found near the turbulent and non-turbulent (jet and non-jet domain) interface of the fluid. There is another cluster of particles that are closer to the centerline. These particle

clusters exist in the areas where the velocity (or) scalar concentration is higher than the surrounding fluid and their gradients are very small.

In the centerline plane, the basic statistical analysis was done on various fluid and particles velocity and the scalar concentration. There is no significant difference in the scalar concentration decay for different St and this decay has the virtual origin at $\sim 2.02t_e$ and converge at 0.2 units. The variance of the scalar concentration has the peak at $\sim 10t_e$ and converge to the value of 0.01 units, irrespective of the St . The scalar mixture fraction variance increases till $St = 1$, compared to the particle-free and higher St , indicating that an optimal St exists for which the scalar variation is maximum.

The fluid velocity of the particle-laden jets decreases at the start due to the transfer of momentum to the particles. The velocity decay when once the flow crosses the transient state is same irrespective of the St . In similar lines of scalar concentration, the velocity converges to the value of $0.15u_{f,a}$. The TKE_f profiles for different St have the peak at $\sim 12t_e$. Just like the scalar variance case, the TKE_f profile for $St = 1$ has later peak and significantly more magnitude around the peak, compared to the particle-free and higher St , indicating that an optimal St exists for which the values around the peak are maximum when compared to other values. The final convergence value of TKE_f plots is $\sim 0.02u_{f,a}^2$.

For the particle's velocity, the lower St follows the fluid profile and attains the fluid velocity much faster when compared to that of higher St , but ultimately irrespective of the St all the velocity and TKE_p converge to the same value of the respective fluid counterparts which are $0.15u_{f,a}$ and $0.02u_{f,a}^2$ respectively. Also, from the TKE_p results, it can be

inferred that the particles can freely absorb and give away the energy from and to the fluid domain for the smaller St whereas it becomes increasingly difficult with increase in St .

In the streamwise-normal plane, the difference between the profiles of mixture fraction among the different St grows and becomes significance as t progresses. Although the difference of scalar concentration profile between different St grows, the position where the maximum occurs is the same which is at the centerline. For the scalar variance, the maximum occurs at the jet concentration half-width, and this is also almost same irrespective of St and t . The peak value of the variance decreases with increase in St . The variance curve from the centerline to the peak is shifted downwards and the slope of the variance curve from peak to the boundary decreases with increase in St .

Although in the fluid velocity profiles, no significant difference is observed for different St , there exists a significant difference at the regions near the boundaries in between the particles and no-particles case due to the significance of the pressure term in solving the particles transport equation during early time steps of the simulation. Same impact can also be observed in the estimation of the TKE_p and R_{uv} at the regions near the boundaries. Also, their respective values for given t is maximum for $St = 1$. This suggests that $St = 1$ case is better when compared to the lower and higher St .

Hence whether streamwise parallel (or) streamwise normal plane is considered, the scalar concentration variance, TKE_f and R_{uv} are comparatively high for $St = 1$ when compared to other St that are away from $St = 1$. This implies that for $St = 1$ effective exchange of turbulence between the particles and fluid occurs causing more scalar variance

and ultimately effective mixing. Also, the jet spread could be noticed when the scalar concentrations are considered. The jet spreading along the width is less common in-case of $St = 1$ when compared with other St . This implies the effective mixing for $St = 1$ within lesser space when compared to other St .

From all the results, the trends of self-similarity can be noticed after a certain time of around $7t_e$. The deviation from the self-similarity can be due to either the velocity or the scalar concentration profile. From the generated and analyzed data, the deviation from the self-similarity in-case of velocity occurs much later than the scalar concentration. For larger St , the deviation from the self-similarity occurs sooner in-comparison to that of lower St . In the current work, as $St = 1$ & $St = 20$ are the most discussed, the deviation from the self-similarity for $St = 20$ occurs around $\sim 30t_e$. For lower St which is $St = 1$, the velocity profiles are self-similar from $10t_e$ to $35t_e$. From extrapolating, the estimated the time for the deviation from the self-similarity, it turns out to be at $\sim 54t_e$.

During the $35t_e$ of analysis, the spread for the particle-laden case is less when compared with the particles-free case, making the particles acting as the barrier for the jet spread. The simulations were successful for the $35t_e$, during which the jet is free from the impacts of the domain size and the jet passing through the cross-sectional boundary. Hence in future studies, the cross-sectional domain length needs to be increased so that the jet can attain stability. This change leads to an increase of the grids in the simulation, eventually requesting more processor cores to solve for the DNS.

In this current work, even when the particles are initiated with zero velocity, the pressure term in transport equation imparts little velocity to the particles that are in the non-jet domain. So, in future studies the velocity of the particles inside the jet can be initialized with the velocity of the jet. Also, the future simulations need to be run in such a way that velocity of the fluid and particles in the non-jet domain at the domain boundaries isn't impacted significantly by the pressure term as in the current work.

Also in the current work, the jet velocity profile considered is the uniform profile and the noise added on top of it. In the future work, the other jet profiles like Gaussian profile along slot width, uniform profile with sinusoidal noise, gaussian profile with sinusoidal noise can be considered so that the difference in results can be observed for these different jet profiles and their effects with different Stokes numbers.

REFERENCES

- A Borg, J Bolinder, L Fuchs. Simultaneous velocity and concentration measurements in the near field of a turbulent low-pressure jet by digital PIV-PLIF. *Experiments in Fluids*, Vol 31: 140 – 152, 2001.
- A Cimarelli, JP Mollicone, MV Reeuwijk, E De Angelis. Spatially evolving cascades in temporal planar jets. *Journal of fluid Mechanics*, Vol 910: A19, 2021
- A Cimarelli, JP Mollicone, MV Reeuwijk, E De Angelis. Structure of turbulence in the temporal planar jets. *Physics of Fluids*, Vol 34: 045109, 2022
- AKMF Hussain. Coherent structures and turbulence. *Journal of Fluid Mechanics*, Vol 173: 303 – 356, 1986.
- CB Da Silva, JCF Pereira. The effect of subgrid-scale models on the vortices computed from large-eddy simulations. *Physics of Fluids*, Vol 16: 4506 – 4534, 2004.
- CWV Atta, P Tabeling, O Cardoso. Shear Flows, Turbulence: A Tentative Dictionary. *Plenum Press*, 1995.
- EK Longmire, K Eaton. Structure of particle-laden round jet. *Journal of Fluid Mechanics*, Vol 236: 217 – 257, 1992.
- F Picano, G Sardina, P Gaultieri, CM Casciola. Particle-laden jets: Particle distribution and back-reaction on the flow. *Journal of Physics: Conference Series*, Vol 318, 2011.
- FH Harlow, JE Welch. Numerical Calculation of Time-Dependent Viscous Incompressible Flow of Fluid with Free Surface. *The Physics of Fluids*, Vol 8(12): 2182 – 2189, 1965.
- JO Hinze. Turbulence 2nd edition. *McGraw-Hill*, 1975.

- J Capecehatro, O Desjardins. A Euler-Lagrange strategy for simulating particle-laden flows. *Journal of Computational Physics*, Vol 238: 1 – 31, 2013.
- J Capecehatro, O Desjardins, RO Fox. Investigating Multiphase turbulence statistics for large-scale two-way coupled gravity-driven flows. *The American Society of Mechanical Engineers*, Summer edition, 2014.
- J Mathieu, J Scott. An Introduction to Turbulent Flow. *Cambridge Press*, 2000.
- K Luo, N Gui, J Fan, K Cen. Direct numerical simulation of a two-phase three-dimensional planar jet. *International Journal of Heat and Mass transfer*, Vol 64: 155 – 161, 2013.
- M Hayashi, T Watanabe, K Nagata. Characteristics of small-scale shear layers in a temporally evolving planar jet. *Journal of Fluid Mechanics*, Vol 920: A38, 2021.
- BK Reville, N Harnby. Mixing in the Process Industries, *Butterworth-Heinemann*, 1997.
- O Desjardins, G Blanquart, G Balarac, H Pitsch. High order conservative finite difference scheme for variable density low Mach number turbulent flows. *Journal of Computational Physics*, Vol 227: 7125 – 7159, 2008.
- P Sagaut, S Deck. Multiscale And Multiresolution Approaches in Turbulence: LES, DES and Hybrid RANS/LES Methods - Applications and Guidelines 2nd edition. *World Scientific Publishing Company*, 2013.
- PA Durbin, BA Petterson Reif. Statistical Theory and Modeling for Turbulent Flows. *John Wiley & Sons*, 2001.
- PA Davidson. Turbulence: An Introduction for Scientists and Engineers. *Oxford University Press*, 2004.

- PJ Ireland, O Desjardins. Improving particle drag predictions in the Euler – Lagrange simulations with two – way coupling. *Journal of Computational Physics*, Vol 338: 405 – 430, 2017.
- R Akhavan, A Ansari, S Kang, N Mangiavacchi. Subgrid-scale interactions in a numerically simulated planar turbulent jet and implications for modelling. *Journal of Fluid Mechanics*, Vol 408: 83 – 120, 2000.
- RA Antonia, BR Satyaprakash, AKMF Hussain. Measurements of dissipation rate and some other characteristics of turbulent plane and circular jets. *The Physics of Fluids*, Vol 23(4): 695 – 700, 1980.
- RN Parthasarathy, GM Faeth. Structure of Particle-laden turbulent water jets in still water. *International Journal of Multiphase Flows*, Vol 13(5): 699 – 716, 1987.
- RR Taveria, CB Da Silva. Characteristics of the viscous superlayer in a shear free turbulence and in planar turbulent jets. *Physics of Fluids*, Vol 26: 021702, 2014.
- SB Pope. *Turbulent Flows*. Cambridge University Press, 2000.
- S Balachandar. A scaling analysis for point-particle approaches to turbulent multiphase flows. *International Journal of Multiphase Flow*, Vol 35: 801 – 810, 2009.
- S Balachandar, JK Eaton. Turbulent Dispersed Multiphase Flow. *Annual Review of Fluid Mechanics*, 42nd edition: 111 – 133, 2010.
- S Corrsin, AL Kistler. Free-stream boundaries of Turbulent Flows. *National Advisory Committee for Aeronautics*, Report 1244: 1 – 32, 1955.
- S Elghobashi, T Abou-arab, M Rizk, A Mostafa. Prediction of the particle-laden jet with a two-equation turbulence model. *International Journal of Multiphase Flow*, Vol 10: 697 – 710, 1984.

S Tenneti, R Gard, S Subramaniam. Drag law for monodisperse gas – solid systems using particle – resolved direct numerical simulation of flow past fixed assemblies of spheres. *International Journal of Multiphase Flow*, Vol 37: 1072 – 1092, 2011.

T Watanabe, X Zhang, K Nagata. Turbulent/Non-turbulent interfaces detected in the DNS of the incompressible turbulent boundary layers. *Physics of Fluids*, Vol 30: 035102, 2018.

Y Morinishi, TS Lund, OV Vasilyev, P Moin. Fully Conservative Higher Order Finite Difference Schemes for Incompressible Flow. *Journal of Computational Physics*, Vol 143(1): 90 – 124, 1998.